From: FNALD::CAROL 14-MAR-1994 06:34:02.10
To: @CDF_ELECT_DIST.DIS
CC:
Subj: CDF Note No. 2435 Now Available as a PostScript File!

March 14, 1994

Dear CDF Collaborators,

CDF Note No. CDF/ANAL/EXOTIC/CDFR/2435, Version 1.0, entitled, "Search for t -> H^+b in the Dilepton Channel," written by J. Wang, X. Wu, M. Contreras, and A. Clark is being distributed. This note can be found in and printed from CDF$PUB:CDFNOTE_2435.PS and CDF$PUB:CDFNOTE_2435_FIG.PS.

Jinsong Wang will present the physics analysis written up in this note for "preblessing" at the Exotic Physics Group Meeting, Thursday, March 17; "blessing" will be asked at the Exotic Physics Group Meeting, Thursday, March 31, and at the CDF Group Meeting, Friday, April 1.

Jinsong Wang

CDF/ANAL/EXOTIC/2435
March 10, 1994
version 1.0

Search for $t \rightarrow H^+ b$ in the Dilepton Channel

Jinsong Wang[1], Xin Wu[2], Milciades Contreras[1], Allan Clark[2]

[1] *University of Chicago,* [2] *University of Geneva*

Abstract

In this note we describe a search for top to charged Higgs decays in the dilepton channel(ee, $\mu\mu$ and $e\mu$ final states) using data from the 1992-93 run. At the Tevatron, where top quarks are generated in pairs, we have three possible types of top decay modes: 1) $t\bar{t} \rightarrow HbHb$, 2) $t\bar{t} \rightarrow HbWb$ and 3) $t\bar{t} \rightarrow WbWb$. In our data sample of 21.6 pb^{-1}, we observe 2 dilepton events with a background estimation of 3.3±1.0 events. Limit at 95% CL in the (M_{top},M_{Higgs}) plane are presented.

1 Introduction

We have conducted a search for top to charged Higgs decays in the dilepton channel. The data used for this search were collected with inclusive electron and inclusive muon triggers in CDF run 1a with an integrated luminosity of 21.6 pb^{-1}.

If a charged Higgs exists and it is lighter than the top quark, then the decay of the top into a charged Higgs boson and a bottom quark could be important. There are two cases defined by whether or not the top quark is heavy enough for an on-shell decay $t \to W^+ b$. In the first case, $m_t < m_W + m_b$, the decay of $t \to H^+ b$ has 100% branching ratio. CDF has conducted a search for the charged Higgs in this case using the 88-89 data in the τ jet analysis[1]. The limits in the (m_t, m_H) plane are shown in Figure 1 and Figure 2. The lower bound of the top mass limit from the measurement of the W width has been improved from 55 GeV to 62 GeV since then[2]. In the second case, $m_t > m_W + m_b$, which is the case that we concentrated on, two competing decay channels of top are open, $t \to W^+ b$ and $t \to H^+ b$. The branching ratio of $t \to H^+ b$ is model dependent, and in general is a function of quark mass, Higgs mass and $tan\beta$ ($tan\beta$ is the ratio of the vacuum expectation values of the two Higgs doublets). Figure 3 shows the branching ratios Br($t \to H^+ b$) and Br($t \to W^+ b$) in the case of the Minimum Supersymmetry Standard Model(MSSM), as a function of $tan\beta$, for two possible m_t and m_H combinations.

At the Tevatron, where top quarks are generated in pairs, we would then have three possible types of top decay modes: 1) $t\bar{t} \to HbHb$, 2) $t\bar{t} \to HbWb$ and 3) $t\bar{t} \to WbWb$.

The decay channels for a charged Higgs lighter than top are mainly $H \to \tau\nu_\tau$ and $H \to c\bar{s}$, with branching ratios varying as a function of $tan\beta$ (see Figure 4). In this search, we are sensitive to large branching ratio of charged Higgs decay to $\tau\nu_\tau$, corresponding to $tan\beta$ above 1 in the MSSM. For τ decays, our search uses only the τ leptonic decay modes, with a total branching ratio of 36%. The branching ratio of $t\bar{t} \to ll b\bar{b}$+X as a function of $tan\beta$ is shown in Figure 5, where the lepton can come either from $W \to l\nu$ or from $H \to \tau\nu_\tau \to l\nu\nu\nu$.

Since leptons from $H \to \tau\nu_\tau \to l\nu\nu\nu$ are much softer than those from $W \to l\nu$, the standard top dilepton search which requires $P_T^l > 20$ GeV has very small sensitivity to the decay mode of top to charged Higgs. This can be seen in the distribution of P_T^l for $t\bar{t} \to HbHb \to ll + X$ in Figure 6. Therefore a separate search with a lower P_T^l cut is necessary. Except for the lower lepton P_T the event topology is similar to standard top events. In Figure 6, we plot the P_T^l of leptons decayed from τ's or b quarks separately for two possible m_t and m_H combinations. When m_t is very close to m_H, the P_T^l of leptons from b decays is soft and when $m_t >> m_H$, the P_T^l of leptons from b decays becomes stiffer. So our signal dileptons are mainly from $\tau\tau \to ll$+X with some contribution of $\tau b \to ll$+X. The distributions of several reconstructed variables from the the signal monte carlo sample are shown in Figure 7a, 7b, 7c, 7d, 7e, 7f, 7g, 7h for m_t = 100 GeV and m_H = 80 GeV. For the signal, we use ISAJET+QFL monte carlo events, with both Br($t \to H^+ b$) and Br($H \to \tau\nu_\tau$) equal 100%. The isolation distributions for the signal Monte Carlo with three mass combinations for $t\bar{t} \to HbHb$ and $t\bar{t} \to WbWb$ are shown in Figure 8 with the comparison of the $b\bar{b}$ background isolation distribution in Figure 9. From Figure 8a,8b and 8c, we can see that when m_t is very close to m_H(e.g. m_t = 100 GeV and m_H = 95 GeV), the

two leptons are both isolated since they come from τ decays. When $m_t >> m_H$(e.g. m_t = 100 GeV and m_H = 65 GeV), there are more non-isolated leptons since there are more leptons from the b quark decays.

Known sources of dilepton events produced at the Tevatron are the following:

$Z \rightarrow e^+e^-, \mu^+\mu^-$; $J/\psi \rightarrow e^+e^-, \mu^+\mu^-$, $\Upsilon \rightarrow e^+e^-, \mu^+\mu^-$; Continuum Drell-Yan; $Z \rightarrow \tau\tau$; QCD heavy flavor production of $b\bar{b}$ or $c\bar{c}$; W + misidentified leptons from QCD jets or hadron decay. The backgrounds are selected against by cuts on the event topology.

In the following sections, we will discuss the following topics:

Dilepton data sample selection; Topology cuts; Acceptance for signal; Background expectation; Conclusions.

2 Dilepton Data Sample

We select our dilepton sample from the stream 1 inclusive lepton data (6.1 production). The total integrated luminosity of the data sample is about 21.6 pb^{-1}.

We demand at least one lepton with $P_T > 9$ GeV and a second lepton with $P_T > 6$ GeV. We call it (9,6) dilepton P_T cut. Only central leptons (CEM and CMUO) are used. The lepton identification cuts are given below.

Identification Cuts for Central Electrons:

E/P	<	1.5
HAD/EM(3 tower)	<	0.05
L_{shr}	<	0.2
χ^2(strip)	<	10
Δx	<	3.0 cm
Δz	<	5.0 cm

Fiducial cuts (C$ELE:FIDELE) and a conversion removal algorithm (C$ELE:CONVERT) are also applied.

Identification Cuts for CMUO Muons:

EM	<	2 GeV
HAD	<	5 GeV
EM+HAD	>	0.1 GeV
Impact parameter d0	<	3 mm
Z vertex match	<	5 cm

We also require at least one of the following: a 10 cm track match to a CMU stub, a 15 cm match to a CMP stub, or a 15 cm match to a CMX stub.

The dilepton sample consists of the events containing at least two leptons that pass the above P_T and identification requirements. We require the event vertex to be within 60 cm of the interaction point in order to avoid badly measured $\not\!\!E_T$. Also, we remove $\mu\mu$ events which are back-to-back within 0.5° in azimuth and 0.1 in pseudo-rapidity on the ground that they are likely to be cosmic rays.

The dilepton P_T^l distribution is shown in Figure 10a.

The distributions of the invariant mass of the two leptons after the ID selection cuts are also shown in Figure 10, separated into the three cases: ee, $\mu\mu$ and $e\mu$. The mass peaks of Z^0, J/ψ and Υ in the ee and $\mu\mu$ channels, as well as the trigger threshold in all three channels, are clearly seen. The invariant mass distribution of $e\mu$ events shows a peak at the low mass end, which is mostly dileptons from sequential bottom quark decays.

After ID cuts, we are left with 8503 events. We will refer to this sample as the dilepton sample. We show, in Figure 11, the distributions of several variables of the dilepton sample which we will use later.

Here we introduce some definitions used in this analysis:

- lepton 1: highest P_T lepton
- lepton 2: second highest P_T lepton
- P_T^{l1}: P_T (E_T in case of electron) of lepton 1
- P_T^{l2}: P_T (E_T in case of electron) of lepton 2
- $\not\!\!E_T$: missing transverse energy corrected for all minimum ionizing (passing EM and HAD energy deposition cuts) muons which pass the muon ID cuts with $P_T>$ 6 GeV, but not corrected for jet energy
- $\sigma(\not\!\!E_T)$: $\not\!\!E_T$ significance defined as $\not\!\!E_T$ divided by the square root of the total sum E_T of the event.
- E_{cone}^{iso}: isolation of lepton, which is the sum of E_T(in GeV) deposited in a cone of 0.4 around the lepton(excluding the E_T^l)
- E_{cone}^{iso1}: isolation of lepton 1
- E_{cone}^{iso2}: isolation of lepton 2
- $\Delta\phi_{\nu l1}$: $\Delta\phi$ between $\not\!\!E_T$and lepton 1
- $\Delta\phi_{\nu l}$: $\Delta\phi$ between $\not\!\!E_T$and the closest lepton
- $\Delta\phi_{\nu jet}$: $\Delta\phi$ between $\not\!\!E_T$and the closest jet

3 Topology cuts

We have studied the signal and backgrounds using various data and MC samples. For signal, we use the ISAJET event generator (modified for top to charged Higgs decay) and QFL detector simulation. For the background of $Z \rightarrow \tau\tau$, we use a $Z \rightarrow ee$ sample from data with the electrons replaced by simulated τ's. For the DY background we use the Z^0 sample to study the event topology. For $b\bar{b}$ and $c\bar{c}$, we use ISAJET+QFL simulation and normalize the number to the data. For fake leptons, we use the same fake calculation technique as the high P_T dilepton analysis. ISAJET + QFL simulated samples are also used for WW processes. The details of these background studies are given in section 5. Here we briefly explain the cuts we have chosen to use after looking at the signal and background Monte Carlo.

1. isolation cut: one lepton $E^{iso}_{cone} < 2$ GeV and the other lepton $E^{iso}_{cone} < 8$ GeV

   Most of the leptons from $b\bar{b}$ or $c\bar{c}$ decays, as well as fake leptons, are not isolated. On the contrary, leptons from top to charged Higgs to τ decays are usually well isolated. But we also expect some fraction of signal events to have one of the leptons originate from semileptonic b decays. Thus, by comparing the isolation distribution of the signal Monte Carlo (figure 8) and the $b\bar{b}$ background isolation distribution(figure 9), we choose our isolation cut as above.

2. mass cut: For ee and $\mu\mu$ events we remove the J/ψ, Υ, low mass Drell-Yan and b sequential decays by requiring $M_{ee,\mu\mu} > 12$ GeV and remove the Z^0 by cutting on $70 < M_{ee,\mu\mu} < 110$ GeV. For $e\mu$ events, we use a cut of $M_{e\mu} > 10$ GeV to remove b sequential decays.

3. $\not\!\!E_T > 20$ GeV, $\sigma(\not\!\!E_T) > 2.4$

   These cuts are very efficient in rejecting several major backgrounds like $b\bar{b}$(see figure 19c, 19d, 19e), $Z \rightarrow \tau\tau$(see figure 16c,16d,16e), Drell-Yan(see figure 17b, 17c, 17d). Given the fact that the background of $b\bar{b}$ is so high without these cuts, we have to choose them although these cuts hurt the signal detection efficiency(see Table 5)

4. W removal: for events in which lepton 1 has $P_T > 25$ GeV and $E^{iso}_{cone} < 2$ GeV, we require $\Delta\phi_{\nu l1} < 165^o$

   This cut is effective in reducing the W + misidentified lepton background since the high P_T lepton and the $\not\!\!E_T$ tend to be back-to-back in the transverse plane of W events(see figure 21). Also from the $Z \rightarrow \tau\tau$ background study, we learned that this cut efficiently suppresses the $Z \rightarrow \tau\tau$ background(see figure 16f and Table 21).

5. $\Delta\phi_{\nu jet} > 30^o$

   This cut is to reject events in which the mismeasurement of jets produces a large $\not\!\!E_T$. In this case the $\not\!\!E_T$ tends to point to the direction of the mismeasured jet. By looking at the Z + jets sample(figure 17h), this cut is efficient in rejecting Drell-Yan background. For this cut, we use the two highest E_T jets in the events satisfying $E_T > 10$ GeV and $|\eta| < 2.4$.

	Run 46518 Charge	Event 16303 E_T (GeV/c)	η	ϕ (deg)
Central electron	+	11.6	0.89	142
Central electron	−	10.7	−0.22	184
Jet 1		44.8	0.08	232
Jet 2		43.8	1.59	158
Jet 3		13.0	2.86	158
MET(Corrected)		100.5		0
$\Delta\phi$ ($\not\!\!E_T$,lepton)				144
$\Delta\phi$ ($\not\!\!E_T$,jet)				128

Table 1: Characteristics of the ee event. Jet energy is the raw calorimeter energy deposited in a cone of 0.4.

6. $\Delta\phi_{\nu l} > 30^o$

   This cut is primarily used to reject $Z \rightarrow \tau\tau$ events since the neutrinos and the lepton from the τ decay tend to point in the the same direction(see figure 16h and Table 21).

The distributions of E_{cone}^{isol} vs E_{cone}^{iso2}, $\not\!\!E_T$, $\sigma(\not\!\!E_T)$, $\sigma(\not\!\!E_T)$ vs $\not\!\!E_T$ are shown in Figure 11a, 11b, 11c, 11d. And after cuts 1,2,3 and 4, the $\Delta\phi(\not\!\!E_T$-lepton or jet) vs $\not\!\!E_T$ distribution is shown in Figure 11h. In Figure 11h we can see that after all topology cuts, we have two candidate events left in our data sample.

4 Comments on the candidate events

One of the two candidate events is the same CEMX event as that in the top dilepton analysis[3] and is described in detail in CDF-1975, Page 14.

The other event(R46518/E16303) is an ee event with 100 GeV $\not\!\!E_T$. The azimuthal angle separation between the positron (with $E_T = 11.6$ GeV) and the electron (with $E_T = 10.7$ GeV) is 42°. There are 3 jets in this events, with raw E_T's of 45, 44 and 13 GeV. The characteristics of the ee event are summarized in Table 1.

The DPF event in the top dilepton analysis[3] failed our isolation requirement. Therefore it's not in our signal region.

5 Acceptance of Signal

The number of top events expected in the data sample can be written as

$$N_{exp} = \int L \cdot dt \cdot \sigma_{t\bar{t}} \cdot BR \cdot \varepsilon_{total}$$

where BR is the branching ratio for $t\bar{t}$ decay to ee, $\mu\mu$ or $e\mu$, and is a function of m_t, m_H and $tan\beta$. The total detection efficiency is decomposed into the following parts:

- $\varepsilon_{geom \cdot P_T}$: the geometric acceptance of the detector and the efficiency of E_T (P_T) cuts
- ε_{event}: the efficiency of event topology cuts(listed in section 3)
- ε_{id}: the efficiencies of electron and muon identification
- ε_{trig}: the trigger efficiencies

Thus $\varepsilon_{total} = \varepsilon_{geom \cdot P_T} \varepsilon_{event} \varepsilon_{id} \varepsilon_{trig}$

We determine $\varepsilon_{geom \cdot P_T}$ and ε_{event} by Monte Carlo simulation, a straight forward calculation. The ID efficiencies ε_{id} are calculated by using J/ψ and Z^0 data for isolated and semi-isolated leptons separately. The trigger efficiencies ε_{trig} are also determined from data.

5.1 Acceptance from Monte Carlo

We modified ISAJET to accommodate top to charged Higgs decays, including assigning the correct helicity to τ's from Higgs decays(Helicity $= -1$ for $H^+ \rightarrow \tau^+ \nu_\tau$). For a given M_t and M_H combination, we simulated three processes: $t\bar{t} \rightarrow HbHb$, $t\bar{t} \rightarrow HbWb$ and $t\bar{t} \rightarrow WbWb$. We call these HH, HW, and WW events. The actual acceptance for a given $tan\beta$ is then obtained by adding these three contributions with appropriate weights.

For each process(HH,HW or WW), we consider two contributions. First is the Boson-Boson contribution which is when both leptons come from Boson (Higgs or W) decays. Second is the Boson-b contribution which is when one of the two leptons comes from a Boson (Higgs or W) decay and the other lepton comes from a b decay.

We simulate the ISAJET events with QFL. Then we apply our dilepton selection cuts, ie. two central leptons with the (9,6) P_T cut. The lepton ID cuts are not used, except the fiducial cut for electrons. However each lepton is required to be matched to a Monte Carlo lepton track by using the down-link OBSP bank number in the corresponding TRKL bank.

The number of events passing the above dilepton selection cuts divided by the total number of $t\bar{t}$ events generated gives $BR \cdot \varepsilon_{geom \cdot P_T}$. These numbers are listed in Table 2 for the Boson-Boson contribution and Table 3 for the Boson-b contribution with different m_t and m_H combinations. The errors in this section are statistical only. Then the topology cut is applied. The number of events passing all the cuts, divided by the number of events passing the dilepton selection cuts gives ε_{event}. We list the event topology cut efficiencies for dileptons from the Boson-Boson contribution and from the Boson-b contribution separately in Table 2 and Table 3. The total $BR \cdot \varepsilon_{geom \cdot P_T}$ and ε_{event} are summarized in Table 4. We also list in Table 4 the

M_{top}	100 GeV						
M_{Higgs}	-	65 GeV		80 GeV		95 GeV	
TYPE	WW	HH	HW	HH	HW	HH	HW
BR_1	0.069	0.13	0.094	0.13	0.094	0.13	0.094
$BR_1 \cdot \varepsilon_{g_1}(\%)$	1.52±0.09	1.65±0.05	1.57±0.05	1.94±0.06	1.61±0.05	2.31±0.06	2.21±0.06
$\varepsilon_1(\%)$	34.2±3.4	26.5±1.6	32.9±1.9	29.9±1.6	32.9±1.8	38.3±1.7	37.9±1.9

Table 2: $BR \cdot \varepsilon_{geom \cdot P_T}$ and ε_{event} of the Boson-Boson contribution for $M_{top} = 100$ GeV.
BR_1 and ε_{g_1} are the branching ratio and $\varepsilon_{geom \cdot P_T}$ of the Boson-Boson contribution(both leptons come from Higgs or W decays). The efficiency ε_1 is the topology cut efficiency ε_{event} for dileptons from the Boson-Boson contribution.

M_{top}	100 GeV						
M_{Higgs}	-	65 GeV		80 GeV		95 GeV	
TYPE	WW	HH	HW	HH	HW	HH	HW
$BR_2 \cdot \varepsilon_{g_2}(\%)$	0.71±0.06	2.90±0.08	2.47±0.06	1.94±0.06	1.93±0.06	0.02±0.01	0.70±0.04
$\varepsilon_2(\%)$	15.7±2.0	10.4±0.8	11.3±0.9	15.3±1.2	14.7±1.1	10.8±3.8	15.6±1.6

Table 3: $BR \cdot \varepsilon_{geom \cdot P_T}$ and ε_{event} of the Boson-b contribution for $M_{top} = 100$ GeV.
BR_2 and ε_{g_2} are the branching ratio and $\varepsilon_{geom \cdot P_T}$ of the Boson-b contribution(one of the two leptons comes from Higgs or W decays and the other comes from b decays). The efficiency ε_2 is the topology cut efficiency ε_{event} for dileptons from the Boson-b contribution.

fractions of dilepton events from the Boson-Boson contribution, $F_{Boson-Boson}$, and the fractions of dilepton events from the Boson-b contribution, $F_{Boson-b}$. These fractions are calculated after the event topology cuts.

Table 5 shows the break-down of the efficiencies for each topology cut in the case of $M_{top} =$ 100 GeV, for HH, HW events with $M_{Higgs} = 80$ GeV, and for Standard Model (WW) events. We list the isolation cut efficiency and the total topology cut efficiency for dileptons from the Boson-Boson contribution and from the Boson-b contribution separately in Table 5. We can see that the isolation efficiency for dileptons from the Boson-b contribution is much lower than dileptons from the Boson-Boson contribution.

5.2 Lepton Identification efficiency

5.2.1 Central electron identification efficiency

We measure ε_{id} for electrons using $J/\psi \rightarrow ee$ events (for E_T<20 GeV) and $Z \rightarrow ee$ events (for E_T>20 GeV).

M_{top}	100 GeV						
M_{Higgs}	-	65 GeV		80 GeV		95 GeV	
TYPE	WW	HH	HW	HH	HW	HH	HW
$BR{\cdot}\varepsilon_{geom{\cdot}P_T}(\%)$	2.23±0.11	4.55±0.09	4.04±0.08	3.88±0.08	3.54±0.08	2.31±0.06	2.91±0.07
total $\varepsilon_{event}(\%)$	24.0±1.9	16.2±0.8	19.7±1.0	22.7±1.0	22.9±1.0	36.9±1.6	29.3±1.3
$F_{Boson-Boson}(\%)$	63.8±3.8	59.4±2.4	64.9±2.2	66.2±2.2	64.9±2.2	98.4±0.6	79.5±1.8
$F_{Boson-b}(\%)$	36.2±3.8	40.6±2.4	35.1±2.2	33.8±2.2	35.1±2.2	1.6±0.6	20.5±1.8

Table 4: Total $BR{\cdot}\varepsilon_{geom{\cdot}P_T}$ and total ε_{event} for $M_{top} = 100$ GeV.
$F_{Boson-Boson}$ and $F_{Boson-b}$ are the fractional contributions of dileptons from the Boson-Boson and the Boson-b respectively after the topology cuts.

TYPE	WW	HH	HW
Iso cut for Boson-Boson	0.842±0.058	0.849±0.027	0.820±0.027
Iso cut for Boson-b	0.470±0.048	0.523±0.020	0.437±0.019
mass cut	0.845±0.046	0.883±0.022	0.884±0.035
$\not\!\!E_T$ cut	0.882±0.051	0.708±0.022	0.834±0.033
$\sigma(\not\!\!E_T)$ cut	0.908±0.056	0.888±0.030	0.911±0.037
W removal cut	0.779±0.055	0.825±0.031	0.745±0.029
$\Delta\phi(\not\!\!E_T$-jet) cut	0.851±0.063	0.905±0.035	0.891±0.037
$\Delta\phi$(lepton-$\not\!\!E_T$) cut	0.92±0.072	0.797±0.035	0.843±0.038
ε_1	0.342±0.034	0.299±0.016	0.329±0.018
ε_2	0.157±0.020	0.153±0.012	0.147±0.011
total ε_{event}	0.240±0.019	0.227±0.010	0.229±0.010

Table 5: Topology cut efficiencies for $M_t = 100$ GeV and $M_H = 80$ GeV, where efficiencies ε_1 and ε_2 are the topology cut efficiencies for dileptons from Boson-Boson contribution and Boson-b contribution.

		E_T	>	6 GeV
		P_T	>	4 GeV
0 .75	<	E/P	<	1.5
		HAD/EM (3 towers)	<	0.04
		L_{shr} (2 towers)	<	0.2
		χ^2(strip)	<	10.
		χ^2(wire)	<	15.
		Δx	<	1.5 cm
		Δz	<	3.0 cm
		Fiducial cuts		(C$ELE:FIDELE)
		Remove conversions		(C$ELE:CONVERT)

Table 6: Tight electron selection cuts

First, we select a di-electron sample from the inclusive electron stream, requiring two electrons (EM clusters) present with at least one passing a set of tight ID cuts (Table 6). The invariant mass distributions of the two mass regions of the J/ψ and the Z^0 are shown in Figure 12a and 12b. We then select $J/\psi \rightarrow ee$ events by reconstructing the invariant mass M_{ee} using the two electron tracks, and requiring 2.95 GeV $< M_{ee} <$ 3.25 GeV. The $Z \rightarrow ee$ events are selected by requiring 83 GeV $< M_{ee} <$ 97 GeV, where M_{ee} is calculated from the electron energies. We find 322 $Z \rightarrow ee$ events and 142 $J/\psi \rightarrow ee$ events after these cuts.

We can obtain the efficiency of each ID cut(labelled cut i) by using the following general formula after applying the ID cut i to both legs of the $J/\psi \rightarrow ee$ or $Z \rightarrow ee$ events:

$$\varepsilon_i = (N_{tt} + N_{ti})/(N_{tt} + N_t)$$

where N_{tt} is the number of events with both leptons passing the tight ID cuts, N_{ti} is the number of events with at least one lepton passing the tight cut and the other lepton passing cut i, and N_t is the total number of events with at least one lepton passing the tight cut.

Since we have a tight-loose isolation cut at $E^{iso}_{cone} < 2$ GeV and $E^{iso}_{cone} < 8$ GeV, we calculate efficiency separately for isolated electrons ($E^{iso}_{cone} < 2$ GeV) and semi-isolated electrons (2 GeV $< E^{iso}_{cone} <$ 8 GeV). The efficiency of each individual variable for isolated and semi-isolated electrons is shown in Table 7 and Table 8. The E/P cut efficiency for $Z \rightarrow ee$ is much lower than for $J/\psi \rightarrow ee$ due to the bremsstrahlung effect. The invariant mass of the $Z \rightarrow ee$ events calculated by the electron energies vs. that calculated by the electron tracks is plotted in Figure 13. We can see that some $Z \rightarrow ee$ events have much lower electron P_T than E_T due to the bremsstrahlung effect which gives a lower invariant mass from the tracking than from the calorimeter.

We then calculate the combined efficiencies when applying all the ID cuts at the same time. These efficiencies as functions of electron E_T are shown in Figure 12c and 12d separately for

cut	ϵ from J/ψ(%)	ϵ for Z^0 (%)
E/P<1.5	99.4±0.6	90.7±1.4
HAD/EM<0.05	94.9±1.7	97.6±0.7
L_{shr} <0.2	96.1±1.5	98.3±0.6
χ^2(strip)<10	96.6±1.4	95.7±1.0
Δx<3 cm	97.2±1.2	93.1±1.2
Δz<5 cm	98.3±1.0	98.3±0.8

Table 7: Isolated electron id efficiency of individual variables

cut	ϵ (%)
E/P<1.5	95.8±3.5
HAD/EM<0.05	88.5±4.1
L_{shr} <0.2	87.5±4.2
χ^2(strip)<10	93.8±3.5
Δx<3.0 cm	96.9±3.4
Δz<5.0 cm	91.7±4.0

Table 8: Semi-isolated electron id efficiency of individual variables

	ε_{id}
E_{cone}^{iso}< 2 GeV	83.3±2.9
2 <E_{cone}^{iso}< 8 GeV	78.1±5.6

Table 9: electron identification efficiency

muon type	CMU	CMP	CMU*CMP	CMX
E_{cone}^{iso}< 2, P_T<20	97.7±2.3	93.8±6.1	98.1±1.4	96.2±3.8
E_{cone}^{iso}< 2, P_T>20	90.6±3.3	94.4±5.5	94.2±1.6	93.5±2.6
2 <E_{cone}^{iso}< 8	90.1±5.0	88.9±7.3	95.4±1.8	85.5±5.9

Table 10: muon identification efficiency

isolated electrons and semi-isolated electrons. For the isolated electrons, the ID efficiency in the region E_T < 20 GeV is mostly from $J/\psi \rightarrow ee$ sample and the ID efficiency in the region E_T > 20 GeV is from $Z \rightarrow ee$ sample. The error is calculated from the number of events in each E_T bin before and after ID cuts using the Poisson distribution. Within statistics the efficiencies are rather independent of E_T of the electrons. Therefore we use the values ε_{id} shown in Table 9 for electrons , which are fitted from Figures 12c and 12d.

Due to limited statistics of semi-isolated Z^0 events, we use the efficiency of semi-isolated electrons, 78.1±5.6%, measured from J/ψ events for both E_T<20 GeV and E_T>20 GeV(see Table 9). The P_T distribution of semi-isolated leptons for m_t = 90 GeV, m_H = 55 GeV from the ISAJET Monte Carlo is shown in Figure 14. We can see that the semi-isolated leptons are mostly low P_T leptons.

5.2.2 Central muon identification efficiency

The muon ID efficiency calculation is very simular to the one for the electrons. Here we just give the results in Table 10. CMU represents muon type CMU only and CMP represents muon type CMP only. CMU*CMP represents muon type CMU and CMP (hit both detectors). Due to limited statistics, we use the efficiency of semi-isolated muons measured from J/ψ events for both E_T<20 GeV and E_T>20 GeV(also in Table 10).

5.3 Trigger efficiency

The inclusive CMU/CMP muon trigger efficiencies have been calculated and documented in CDF-2367[5]. Here we quote the results in Table 11. Since the trigger turn-on is around 9 GeV for level 1 and level 2, we use the plots of trigger efficiencies vs. P_T in CDF-2367 to determine

P_T^μ	level 1(%)	level 2(%)	level 3(%)	total(%)
P_T> 11 GeV	95.0±0.8	90.2±1.5	98.0±1.0	84.0±2.0
P_T> 15 GeV	94.7±1.0	93.7±1.5	98.0±1.0	87.0±2.0

Table 11: Muon trigger efficiencies[5].

level 1	level 2	level 3	total
0.992±0.001	0.935±0.003	0.982±0.001	0.911±0.003

Table 12: High E_T electron trigger efficiencies [4].

the muon trigger efficiency near 9 GeV by fitting a curve.

For high E_T (E_T>15 GeV) electrons, we use the trigger efficiency used by the top dilepton analysis[3], as given in Table 12[4]. Electrons with E_T between 9 and 15 GeV are in the level 2 trigger turn-on region, and thus need to be studied separately. We did this study using a dielectron sample from the inclusive electron trigger path, as described in detail below. For level 1 and level 3 efficiencies, we use the same numbers as that in the high E_T case.

A dielectron data sample is selected from events in which both the level 1 and level 2 inclusive electron triggers fired. We then require that there be two and only two electrons passing the ID cuts, and at least one of which passed a tight cut and matched a level 2 inclusive electron cluster. This way the other electron in the event can be considered as unbiased by the triggers and can be used to measure the trigger efficiency. The level 2 inclusive electron trigger efficiency can be then measured by matching the other electron to a level 2 inclusive EM cluster, using the same formula as the one used for the electron ID efficiency calculation (ie. taking into account the cases that both electrons can fire the inclusive electron trigger). The results are summarized in Table 13. The number for high E_T electrons is similar to the one used by the top dilepton analysis. The turn on curve of trigger efficiency vs. E_T is shown in Figure 15 and used to calculate the total detection efficiency.

	$9<E_T^e<10$	$10<E_T^e<11$	$11<E_T^e<12$	$12<E_T^e<15$	$E_T^e>15$
ε_{trig}	0.74±0.03	0.87±0.02	0.92±0.02	0.93±0.01	0.93±0.01

Table 13: Inclusive electron L2 trigger efficiencies.

M_{top}	100 GeV						
M_{Higgs}	-	65 GeV		80 GeV		95 GeV	
TYPE	WW	HH	HW	HH	HW	HH	HW
ε_{id}(%)	78.5±2.4	79.7±2.4	78.9±2.4	79.5±2.4	78.4±2.4	79.0±2.4	78.5±2.4
ε_{trig}(%)	79.7±1.6	78.2±1.6	78.2±1.6	77.6±2.6	81.4±1.6	84.3±1.7	82.8±1.7
$\varepsilon_{id}\cdot\varepsilon_{trig}$(%)	62.6±1.9	62.3±1.9	61.7±1.8	61.7±1.8	63.5±1.9	66.6±2.0	65.0±2.0

Table 14: ε_{id}, ε_{trig} and $\varepsilon_{id}\cdot\varepsilon_{trig}$ for M_{top} = 100 GeV

M_{top}	110 GeV												
M_{Higgs}	-	45 GeV		55 GeV		65 GeV		80 GeV		95 GeV		105 GeV	
TYPE	WW	HH	HW	HH	HW	HH	HW	HH	HW	HH	HW	HH	HW
$BR\cdot\varepsilon_{total}$(%)	0.51	0.31	0.37	0.37	0.47	0.45	0.52	0.53	0.52	0.63	0.54	0.68	0.56
N_{top}	5.8	3.5	4.2	4.3	5.3	5.1	5.9	6.1	6.0	7.2	6.2	7.7	6.4

Table 15: $BR\cdot\varepsilon_{total}$ and number of events expected for M_{top} = 110 GeV. The total fractional uncertainty on each of these numbers is 17%.

5.4 Total acceptance and systematics

The above ID and trigger efficiencies are applied to the signal Monte Carlo events which have passed the topology cuts to obtain ε_{id} and ε_{trig}. The results are listed in Table 14. The product of ε_{id} and ε_{trig} is also listed in the table and is flat for different m_t and m_H combinations with a small increase when m_t is close to m_H. The uncertainties of the numbers in this table are statistical only.

Putting all the acceptance and efficiencies together, we get the total acceptance $BR\cdot\varepsilon_{total}$, given in Table 15, 16, 17, 18 and 19. The number of events expected are also given in Table 15, 16 17, 18 and 19 for 21.6 pb^{-1}. We assume $\sigma_{t\bar{t}}$ = 52.7, 67.3, 86.3, 112 and 148 pb for M_{top} = 110, 105, 100, 95 and 90 GeV respectively [6], which are one σ lower than the central values of the reference. We use the lower end of the range of the theoretical cross sections for the purpose of setting a limit.

The systematic uncertainty on the overall acceptance comes mainly from the modeling of gluon radiation, the detector simulation, and limited Monte Carlo statistics.

One source of systematic uncertainty is the modeling of initial state radiation. Initial state radiation affects the motion of the $t\bar{t}$ system and hence the rapidity and transverse momentum distributions of the top quark decay products. Also, the modeling of gluon radiation affects the isolation properties of the leptons, and hence their topology cut efficiency. This effect can be studied by turning on and off gluon radiation in ISAJET, and taking half the difference in the corresponding efficiencies as an estimate of the systematic uncertainty. The uncertainty of

M_{top}	105 GeV												
M_{Higgs}	-	45 GeV		55 GeV		65 GeV		80 GeV		95 GeV		100 GeV	
TYPE	WW	HH	HW	HH	HW	HH	HW	HH	HW	HH	HW	HH	HW
$BR{\cdot}\varepsilon_{total}(\%)$	0.60	0.33	0.45	0.41	0.43	0.50	0.52	0.59	0.54	0.63	0.53	0.59	0.54
N_{top}	8.7	4.8	6.6	5.9	6.2	7.2	7.6	8.6	7.8	9.2	7.7	8.6	7.9

Table 16: $BR{\cdot}\varepsilon_{total}$ and number of events expected for $M_{top} = 105$ GeV. The total fractional uncertainty on each of these numbers is 17%.

M_{top}	100 GeV										
M_{Higgs}	-	45 GeV		55 GeV		65 GeV		80 GeV		95 GeV	
TYPE	WW	HH	HW	HH	HW	HH	HW	HH	HW	HH	HW
$BR{\cdot}\varepsilon_{total}(\%)$	0.51	0.30	0.38	0.41	0.48	0.46	0.49	0.54	0.52	0.60	0.55
N_{top}	9.6	5.5	7.0	7.6	9.0	8.6	9.2	10.1	9.7	11.2	10.3

Table 17: $BR{\cdot}\varepsilon_{total}$ and number of events expected for $M_{top} = 100$ GeV. The total fractional uncertainty on each of these numbers is 17%.

M_{top}	95 GeV										
M_{Higgs}	-	45 GeV		55 GeV		65 GeV		80 GeV		90 GeV	
TYPE	WW	HH	HW	HH	HW	HH	HW	HH	HW	HH	HW
$BR{\cdot}\varepsilon_{total}(\%)$	0.50	0.31	0.40	0.35	0.45	0.38	0.43	0.54	0.50	0.53	0.56
N_{top}	12.0	7.4	9.7	8.5	10.9	9.2	10.4	13.0	12.2	12.8	13.5

Table 18: $BR{\cdot}\varepsilon_{total}$ and number of events expected for $M_{top} = 95$ GeV. The total fractional uncertainty on each of these numbers is 17%.

M_{top}	90 GeV										
M_{Higgs}	-	45 GeV		55 GeV		65 GeV		80 GeV		85 GeV	
TYPE	WW	HH	HW	HH	HW	HH	HW	HH	HW	HH	HW
$BR{\cdot}\varepsilon_{total}(\%)$	0.42	0.26	0.35	0.34	0.40	0.41	0.43	0.47	0.44	0.55	0.51
N_{top}	13.4	8.2	11.1	10.9	12.9	13.1	13.9	14.9	14.0	16.9	16.2

Table 19: $BR{\cdot}\varepsilon_{total}$ and number of events expected for $M_{top} = 90$ GeV. The total fractional uncertainty on each of these numbers is 17%.

Systematic uncertainty	%
Modeling of Gluon Radiation	8
Trigger Efficiency	2
Identification Efficiency	10
QFL simulation	5
Integrated Luminosity	7
Monte Carlo Statistics	7
Total	17

Table 20: Systematic uncertainty of overall acceptance and efficiency

the efficiency on the modeling of gluon radiation is 8%. Another systematic uncertainty results from the choice of structure functions. This work is still in progress.

The ID efficiency for semi-isolated leptons from b decays is measured from our semi-isolated leptons in the J/ψ data sample. We assign a 20% uncertainty to this measurement. The total uncertainty of the ID efficiency(10% in Table 20) is the sum in quadrature of the statistical uncertainty in Table 9 and 10 folded in with this additional 20% uncertainty on the ID efficiency for dileptons from Boson-b contribution.

Detector simulation also affects lepton identification. Here, we take half the difference between the result obtained from CDFSIM and that obtained from QFL as the uncertainty; this is 5% according to the top dilepton analysis[3]. Monte Carlo simulated with CDFSIM for our sample is still in progress.

Monte Carlo statistical error is about 7% and we'll improve it to less than 5%.

The uncertainty on the luminosity measurement is 7%.

The sum in quadrature of all the uncertainties listed above is 17%. We summarize the uncertainties of the overall acceptance-efficiency in Table 20. These uncertainties are essentially independent of top mass or Higgs mass.

6 Background Expectation

As mentioned in section 1, the main backgrounds in the dilepton sample are $Z \rightarrow \tau\tau$, Drell-Yan, QCD production of $b\bar{b}$ or $c\bar{c}$, and W + misidentified leptons from a QCD jet or hadron decay. There are also contributions from diboson production (WW, WZ). In this section we explain how we estimate the background.

CUT in following order	efficiency
Isolation cut	0.973±0.025
mass cut	0.944±0.026
$\not\!\!E_T$ cut	0.279±0.021
$\sigma(\not\!\!E_T)$ cut	0.814±0.046
W removal cut	0.350±0.033
$\Delta\phi(\not\!\!E_T$-jet) cut	0.934±0.065
$\Delta\phi$(lepton-$\not\!\!E_T$) cut	0.233±0.029
total	0.016±0.003

Table 21: Topology cut efficiencies for $Z \rightarrow \tau\tau$ background.

6.1 $Z \rightarrow \tau\tau$

We have simulated the $Z \rightarrow \tau\tau$ sample from our data sample of 1113 $\gamma/Z^0 \rightarrow ee$ events[7]. We replace the electron with a τ that has the same P_T. The τ is then allowed to decay to electrons or muons. The details of making this $Z \rightarrow \tau\tau$ sample are in CDF note 2108. Figure 16 shows distributions of several reconstructed variables. We use this sample to measure the topology cut efficiencies.

We also generated three ISAJET+QFL samples, each with 30k events and a different value of the parameter QTW(0,3 and 7) which controls the transverse momentum of the Z. These samples are used to get the efficiencies for the geometry, P_T, ID and isolation cuts. We find that these efficiencies for different values of parameter QTW are similar and the difference is within 3%.

The efficiencies for event topology cuts are given in Table 21. You can see that the W removal cut and the $\Delta\phi$(lepton-$\not\!\!E_T$) cut greatly reduce this background after the $\not\!\!E_T$ cut.

For the $Z \rightarrow \tau\tau$ cross section, we use the measured $Z \rightarrow ee$ cross section of 209 pb from the 88-89 data[8] and the branching ratio for $\tau\tau$ to dilepton(ee, $\mu\mu$ or $e\mu$) BR = $(0.178\times2)^2$ = 0.127.

The number of $Z \rightarrow \tau\tau \rightarrow$ dilepton events expected for 21.6 pb^{-1} luminosity is 0.48 ± 0.10. The uncertainty includes statistical and systematic uncertainties.

6.2 Drell-Yan

We use a similar method to estimate this background as that in the top dilepton analysis[9]. We use the observed $Z^0 \rightarrow ee$, and $Z^0 \rightarrow \mu\mu$ distributions to predict the background from the continuum. Our initial assumption is that the $P_T(\gamma/Z^0)$ distributions inside and outside the Z^0 region are similar. ISAJET predicts that there is a slight stiffening of the $P_T(\gamma,Z^0)$ with increasing mass, which could lead to an overestimate of the background.

	Cut	Number of Events	Fraction
a)	Z events	702	100%
b)	$\not\!\!E_T > 20$GeV	33	4.7%
c)	b) + $\sigma(\not\!\!E_T) > 2.4$	18	2.6%
d)	c) + W removal	9	1.3%
e)	d) + $\Delta\phi(\not\!\!E_T$,jet) cut	4	0.6%
f)	e) + $\Delta\phi(\not\!\!E_T, l)$ cut	2	0.3%

Table 22: Topology cut rejections. Each line is an independent cut.

The large $\not\!\!E_T$ in Z^0 events originates frequently from jet mismeasurement. In these cases the direction of the $\not\!\!E_T$ is along one of the jets. To obtain greater rejection against Drell-Yan events we require that the $\not\!\!E_T$ be more than 30 degrees away from the closest jet. Figure 17 shows distributions of several reconstructed variables of the Z sample. From figure 17h, we can see that for events with more than 20 GeV $\not\!\!E_T$, most of them have $\Delta\phi_{\nu jet} < 30^o$.

Table 22 lists the fractions of Z events passing various topology cuts in sequence. After all topology cuts, there are two events left(one ee and one $\mu\mu$) in the Z-region.

The scaling factor from the region inside of the Z window to outside of the Z window is obtained from the ISAJET Monte Carlo sample with only Geometry and P_T cuts. The ISAJET cross section has been scaled down to match the Drell-Yan cross section measured in 88-89 data [10]. We get the scaling factors as follow:

N(12-70 GeV) : N(70-110 GeV) : N(110 GeV above) = 0.95 : 1 : 0.04

The $\not\!\!E_T$ cut efficiencies are very different for Drell-Yan outside the Z mass window and inside the Z mass window. Therefore a correction factor for this efficiency is important. We study this effect by using the ISAJET Monte Carlo sample. In Figure 18, we plot the invariant mass and $\not\!\!E_T$ distributions for Drell-Yan events inside and outside the Z mass window. After the (9,6) dilepton P_T cut, the Drell-Yan outside the Z mass window is dominant by events with mass around 25 GeV(see Figure 18a), the jet activity is much lower than high mass Drell-Yan like Z. We list the $\not\!\!E_T$ cut efficiency for different mass bins in Table 23. The correction factors we get from this ISAJET Monte Carlo are

ε(12-70) : ε(70-110) : ε(>110) = 0.11 : 1 : 2.4

So when we scale the number of events from the region inside of the Z window to the region outside of the Z window, we get the background expectation of 0.38 ± 0.27 events in the signal region.

mass bin(GeV)	12−40	40−70	70−110	110 above
$\epsilon(\not\!\!E_T > 20$ GeV)	0.0030	0.034	0.078	0.20

Table 23: $\not\!\!E_T$ cut efficiencies for different Drell-Yan mass bins from the ISAJET Monte Carlo.

6.3 $b\bar{b}$ or $c\bar{c}$

A dilepton Monte Carlo sample is generated in which the P_T of both leptons must be > 5 GeV. The events are generated using ISAJET with the internal loop turned on to speedup heavy quark production processes. With the multi-evolving technique, ISAJET attempts to simulate the next to leading order (NLO) $b\bar{b}$ production processes such as gluon splitting and flavor excitation. We keep events that have at least two b quarks or gluons with $P_T > 12$ GeV (this corresponds to keeping 90% of the events in which the daughter leptons have $P_T > 5$ GeV). Next, the event is passed through the CLEO MC Module, which redecays the B mesons in the event. This changes the average charged particle multiplicity and energy flow around the lepton (We think that the CLEO B decay package is a better model than ISAJET for B physics). After making the selection cuts at the GENP level (we require that two leptons have P_T greater than 5 GeV/c), we pass the events through the QFL simulation. Figure 19 shows the standard reconstructed variables for this background.

The Monte Carlo is normalized by comparing the $e\mu$ data and the Monte Carlo in the region $M_{e\mu} < 5$ GeV/c^2, where b quark sequential decays dominate. By comparing 686 $e\mu$ data events(21.6 pb^{-1}) and 1034 Monte Carlo events(37.5 pb^{-1}) with the (9,6) dilepton P_T selection, we obtain a normalization factor DATA/MC = 1.2±0.5, where we assign a 40% uncertainty due to the large uncertainty of the ID efficiency of leptons decayed from b quarks in the Monte Carlo and the small uncertainty of the b fraction in the data of the sequential peak. The number of background events from $b\bar{b}$ or $c\bar{c}$ sources to our analysis is estimated as 0.58 ± 0.58 events for a luminosity of 21.6 pb^{-1}.

6.4 WW, WZ

The WW and WZ background samples are generated using ISAJET (6.43) and then are simulated with QFL and reconstructed. The W decay modes we used are $W \to e\nu$, $W \to \mu\nu$ and $W \to \tau\nu$. We generated 10,000 WW events which corresponds to an integrated luminosity of 9469 pb^{-1}. The ISAJET cross-section for WW production, which is 6.0 pb, has been scaled up to match the theoretical calculations given by Ohnemus[11]. We use the calculation from Ohnemus that uses the structure functions HMRSB and has a $\sigma = 9.5$ pb. We assign a theoretical uncertainty of 30% due to the difference of the cross section. Figure 20 shows the standard reconstructed variables for this background.

Event topology efficiencies are shown in Table 24. For a luminosity of 21.6 pb^{-1} we expect

$\sigma \cdot Br$	$\epsilon_{\text{geom}\cdot P_T}$	ϵ_{event}	ϵ_{total}	Number(exp)
0.656	0.220	0.444	0.045	1.02±0.31

Table 24: Expectation for background from the WW $\rightarrow ll$ + X production for 21.6 pb^{-1}

WW,WZ	1.1 ± 0.3
$Z \rightarrow \tau\tau$	0.5 ± 0.1
$b\bar{b}$	0.6 ± 0.6
Drell-Yan	0.4 ± 0.3
Fake lepton	0.8 ± 0.8
Total	3.4 ± 1.1

Table 25: Number of background events expected in 21.6 pb^{-1}

1.02±0.31 events from the WW background, while the contribution from WZ production is only 0.04±0.01 events.

6.5 W+fake

We expect that some of the dilepton events with large $\not\!\!E_T$ are W + jets events where the low P_T lepton is actually a fake lepton. To study this, we apply cuts of $P_T > 25$ GeV, and $E_{cone}^{iso} < 2$ GeV for lepton 1 and $\not\!\!E_T > 20$ GeV to the W + jets sample. There are 142 events that remain. From the transverse mass plot of $\not\!\!E_T$ and P_T^{l1}(Figure 21a), we can see an indication of W events. To remove these events, we use the fact that in W events the lepton and the $\not\!\!E_T$ tend to be back-to-back in the transverse plane, as shown in the scatter plot of $\Delta\phi_{\nu l1}$ vs P_T^{l1}(Figure 21b), where $\Delta\phi_{\nu l1}$ is the azimuthal angle difference between lepton 1 and $\not\!\!E_T$. The $\Delta\phi_{\nu l1}$ distribution of the signal is less back to back (shown in Figure 7f). We calculate the fake probability of electrons and muons from the QCD stream 1 JET20 data. We then multiply the fake probability by the number of W + jet events which survive our event topology cuts to give the estimate of this background. More detailed studies of this background are still in progress.

6.6 Background Summary

The background estimates are summarized in Table 25.

7 Limit on $t\bar{t}$ Production

The $t\bar{t}$ production cross section can be written as :

$$\sigma_{t\bar{t}} = \frac{N_{obs}}{\int \mathcal{L}dt \; Br \; \epsilon_{total}} \quad (1)$$

where N_{obs} is the background subtracted number of observed events, $\int \mathcal{L}dt$ is the integrated luminosity of the data sample, and $Br \cdot \epsilon_{total}$ is the efficiency for observing $t\bar{t}$ events in the selected channel. The uncertainty in ϵ_{total} was discussed at length in section 4.4 and summarized in Table 20. The background subtraction for N_{obs} will be done in the future.

In our data sample of 21.6 pb^{-1}, we observe 2 dilepton events and expect a background of 3.3±1.0 events. Using equation (1) and Table 15, 16, 17, 18, 19, we exclude regions of the (m_t,m_H) plane at 95% confidence level for the case $Br(t \rightarrow H^+ b) = 1.0$ and $Br(H \rightarrow \tau\nu_\tau) = 1.0$ in Figure 22 without background subtraction. Also we show the limit for the case $Br(H \rightarrow \tau\nu_\tau) = 0.75$ and 0.5. In Figure 23, we exclude regions using the two Higgs doublet model which is the simplest non-minimal standard model Higgs structure. The number of events expected for a fixed $tan\beta$ in this model can be written as:

$$N_{exp}(\text{theory}) = N_1 \cdot Br_{t\bar{t}\rightarrow WbWb} + N_2 \cdot Br_{t\bar{t}\rightarrow HbHb} \cdot (Br_{H\rightarrow\tau\nu})^2 + N_3 \cdot Br_{t\bar{t}\rightarrow HbWb} \cdot Br_{H\rightarrow\tau\nu} \quad (2)$$

where N_1, N_2 and N_3 are the numbers of events expected for WW, HH and HW combinations listed in Table 15, 16, 17, 18 and 19. In Table 26, we list the measured upper limits on the $\sigma_{t\bar{t}}$ at 95% CL for different $tan\beta$ values. We also list the theoretical lower limits on the $\sigma_{t\bar{t}}$[6] for different top masses. In Figure 23 we present the limits in the (m_t,m_H) plane for two $tan\beta$ values.

8 Conclusion

We have found no evidence of $t\bar{t}$ production in which the top decays to a charged Higgs. For the case $m_t < m_W + m_b$, we exclude the entire (m_t,m_H) plane where the $Br(H \rightarrow \tau\nu_\tau)$ is large. We also set the limit in the (m_t,m_H) plane for the two Higgs doublet model. The upper limit in the (m_t,m_H) plane has been much improved compared with previous results. For small $tan\beta$ values, we do not have sensitivity because the dominant decay mode of Higgs is $H \rightarrow c\bar{s}$. This produces 6-jet events in $t\bar{t}$ decay, which has a large QCD background.

9 Acknowledgments

We want to thank Mel Shochet and Henry Frisch for a careful reading of this note and for their comments and suggestions.

$tan\beta$	M_{top} (GeV)	M_{Higgs} (GeV)						$\sigma_{t\bar{t}}$(theory) in pb
		45	55	65	80	95	105	
		Cross section limit $\sigma_{t\bar{t}}$ in pb (95% CL)						
	110	25.1	31.1	36.8	43.4	48.7	46.9	52.7
	105	44.3	53.6	65.6	77.1	79.1		67.3
100	100	64.4	88.9	100	117	126		86.3
	95	112	129	139	152			112
	90	163	217	261	295			148
	110	34.9	40.6	43.9	45.1	45.5	45.5	52.7
	105	65.1	67.5	77.8	82.6	85.9		67.3
15	100	86.4	108	114	121	123		86.3
	95	141	162	169	197			112
	90	193	245	281	294			148
	110	42.0	44.1	45.1	45.3	45.4	45.4	52.7
	105	80.0	80.6	84.4	85.9	86.8		67.3
5	100	110	119	121	123	123		86.3
	95	177	188	190	199			112
	90	247	277	292	294			148
	110	35.5	39.6	42.0	43.7	45.0	45.4	52.7
	105	66.8	69.0	76.7	81.9	85.9		67.3
2	100	89.5	105	110	118	123		86.3
	95	142	160	169	193			112
	90	189	229	259	286			148
	110	27.1	31.7	35.3	39.4	43.5	45.2	52.7
	105	49.9	53.6	63.3	73.8	84.0		67.3
1.5	100	64.6	80.6	90.0	108	122		86.3
	95	98.4	118	133	176			112
	90	121	157	195	263			148

Table 26: Measured upper limits on the cross section $\sigma_{t\bar{t}}$ in pb at 95% CL for a given top mass and Higgs mass combination with several $tan\beta$ values. The last column lists the lower limits (at one sigma) of the theoretical $\sigma_{t\bar{t}}$ for different top masses [6].

References

[1] F. Abe, C. Jessop *et al.*, CDF note # 2164, Phy. Rev. Letter preprint.
"A Search for the Top Quark deaying to a Charged Higgs in $p\bar{p}$ Collisions at $\sqrt{s} = 1.8\ TeV$"

[2] F. Abe, S. Kopp *et al.*, CDF note # 2182, submitted to Phy. Rev. Letter.
"Measurement of the Ratio $\sigma B(W \rightarrow e\nu)/\sigma B(Z^0 \rightarrow e^+e^-)$ in $p\bar{p}$ Collisions at $\sqrt{s} = 1.8\ TeV$"

[3] T. Chikamatsu, A. Martin, J. Romano, J. Wang, A. Beretvas, M. Contreras, L. Demortier, H. Frisch, S. Kopp, Y. Seiya, L. Song, L. Stanco, C. Wendt, Q. F. Wang, and G. P. Yeh, CDF Note # 1975 (1993).
"Top Dilepton Analysis"

[4] S. Kopp, CDF Note # 2391 (1993).
" Measurement of the Central Inclusive Electron Trigger Efficiency for the 1992-1993 Run 1A "

[5] Tom LeCompte, Tony Liss, Andrew Martin, CDF Note # 2367 (1993).
"High P_T CMU/CMP Muon Trigger Efficiencies for Run 1A"

[6] E. Laenen, J. Smith and W. van Neerven, Fermilab-Pub-93/270-T, (1993).

[7] J. Wang and M. Contreras, CDF Note # 2108 (1993).
"Estimate of $Z^0 \rightarrow \tau^+\tau^-$ background in the Top Dilepton Analysis"

[8] F. Abe, P. Derwent *et al.* Phy. Rev. D 44, 29 (1991).
"Measurement of $\sigma B(W \rightarrow e\nu)$ and $\sigma B(Z^0 \rightarrow e^+e^-)$ in $p\bar{p}$ collisions at $\sqrt{s} = 1.8$ TeV."

[9] M. Contreras and J. Wang, CDF Note # 2261 (1993).
"Estimate of the Drell-Yan Background in the Top Dilepton Analysis"

[10] F. Abe *et al.* Phy. Rev. D preprint, Third Series, Vol. 49, No. 1.
"Measurement of Drell-Yan electron and muon pair differential cross sections in $p\bar{p}$ collisions at $\sqrt{s} = 1.8$ TeV."

[11] J. Ohnemus, Phys. Rev. D 44, 1403 (1991).

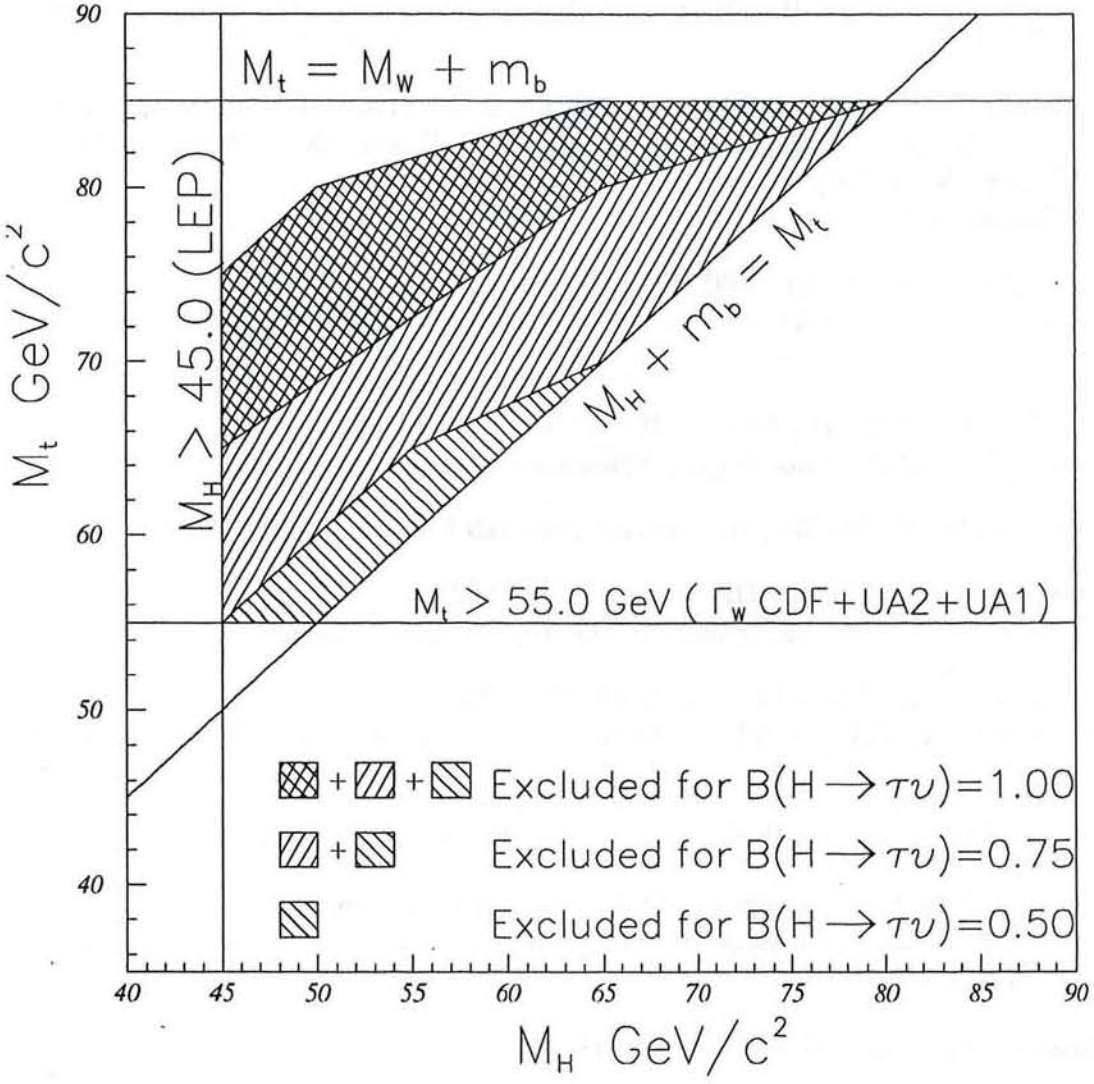

Figure : 1. Regions of (m_t, m_H) plane excluded at 95% CL. for Br($t \rightarrow H^+ b$)=1.0 from the τ jet analysis on the 88-89 data.

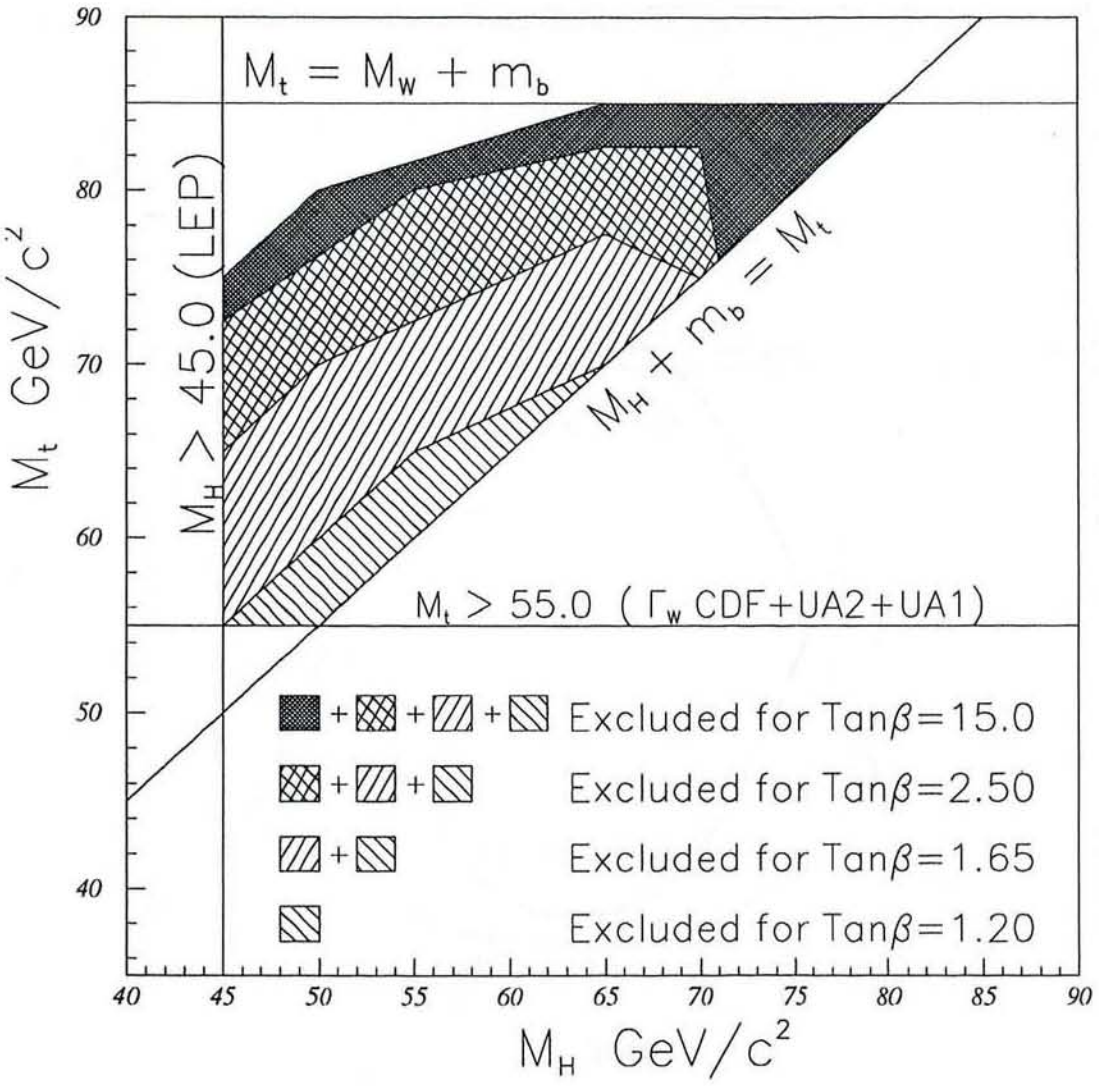

Figure : 2. Regions of (m_t, m_H) plane excluded at 95% CL. for the two Higgs doublet model from the τ jet analysis on the 88-89 data.

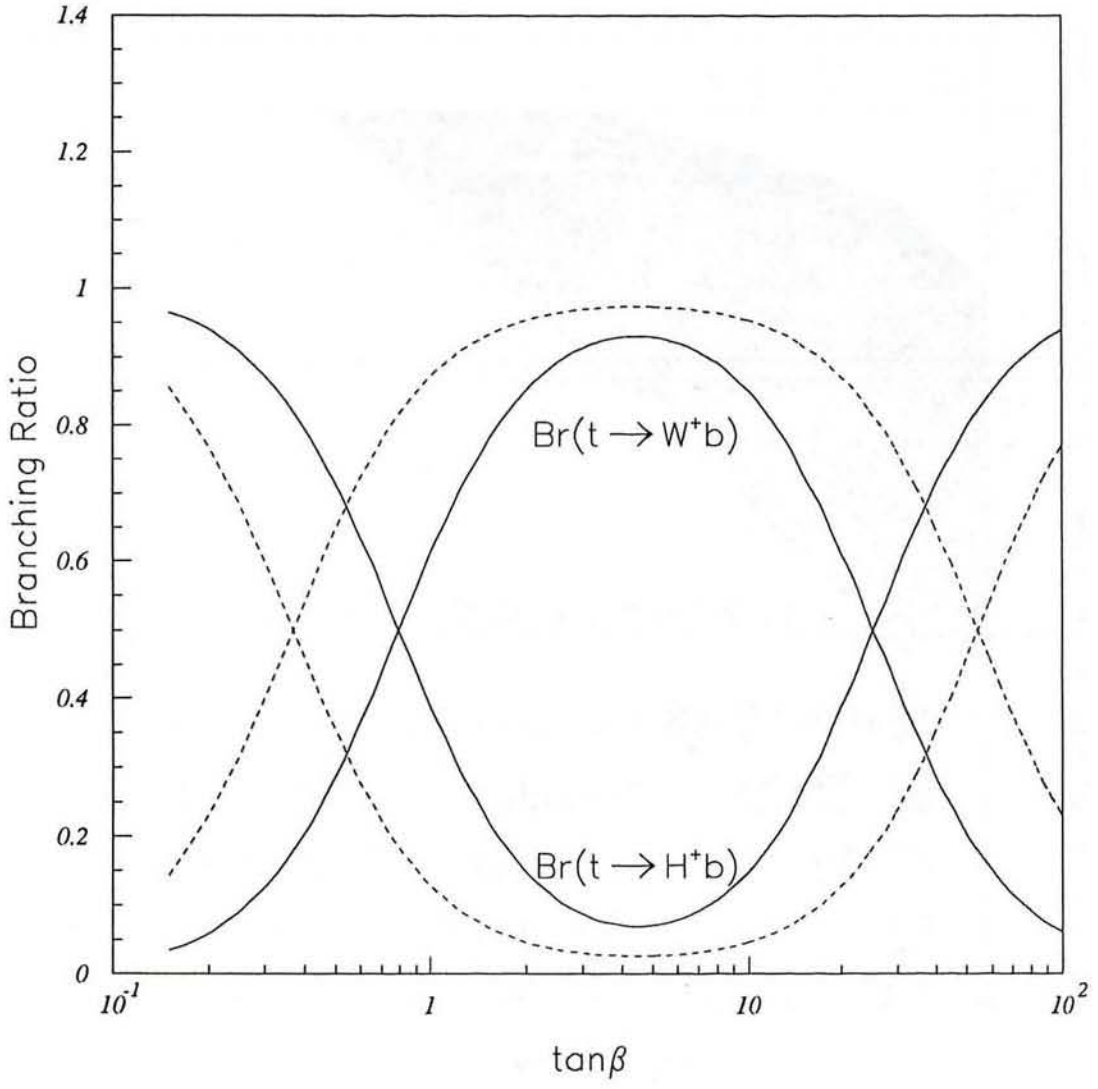

Figure : 3. BR($t \to H^+ b$) and BR($t \to W^+ b$) as a function of $tan\beta$, for two possible m_t and m_H combinations. The solid line is for $m_t = 100$ GeV and $m_H = 70$ GeV; the dashed line is for $m_t = 100$ GeV and $m_H = 95$ GeV.

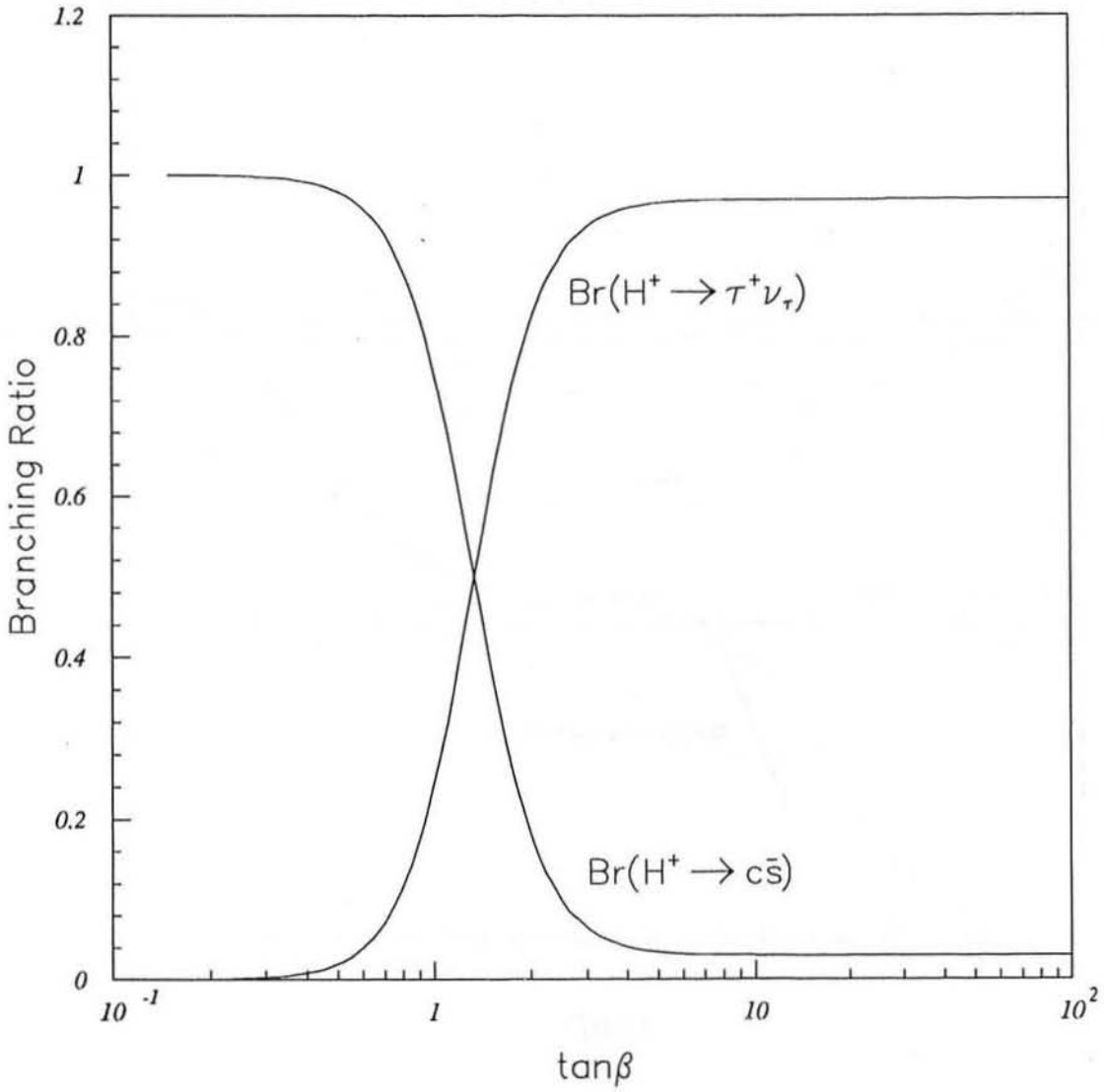

Figure : 4. Branching ratio of $H \rightarrow \tau\nu_\tau$ and $H \rightarrow c\bar{s}$ as a function of $tan\beta$

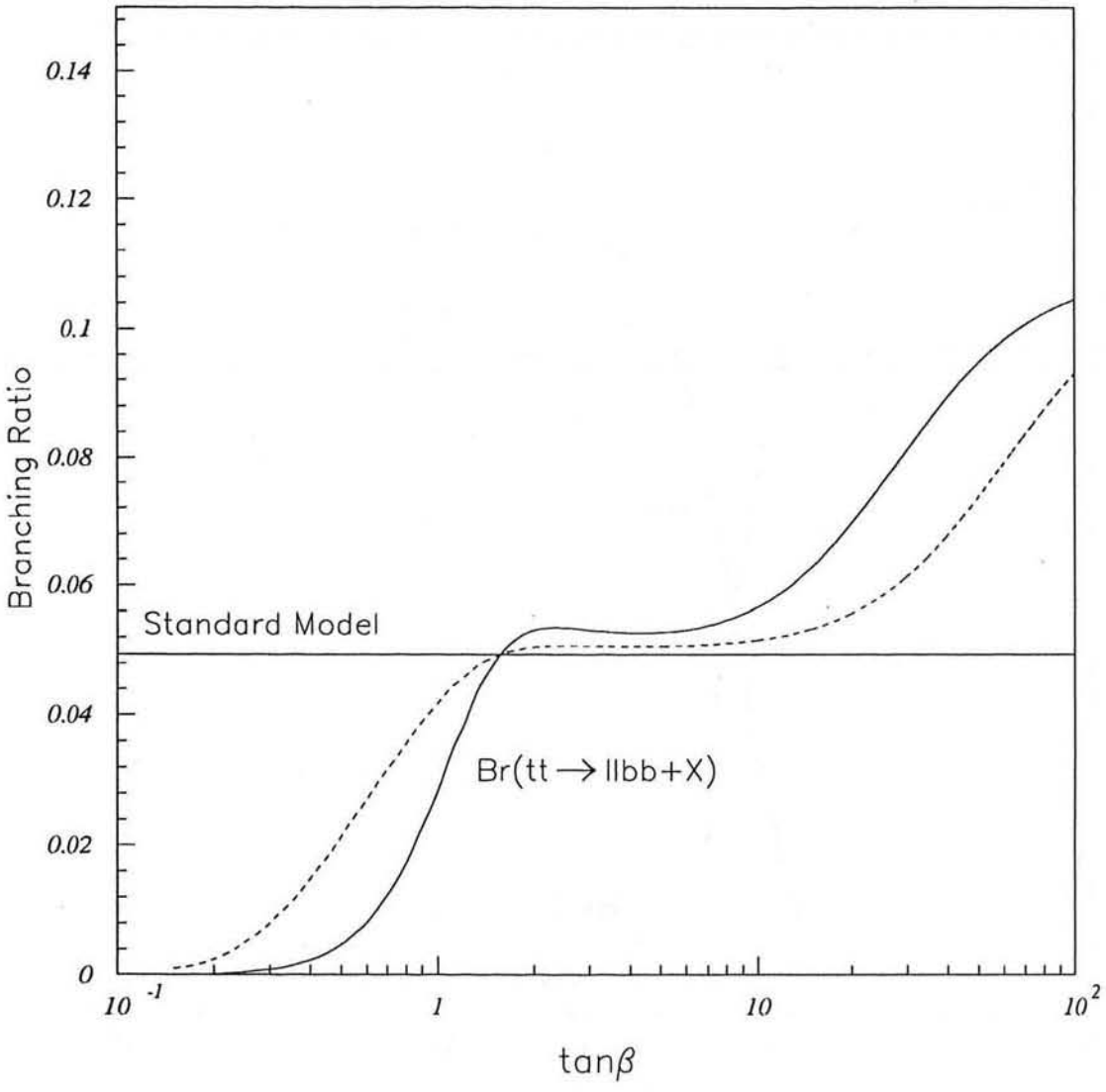

Figure : 5. The branching ratio of $t\bar{t} \rightarrow l l b \bar{b}$+X as a function of $tan\beta$. The solid line is for $m_t = 100$ GeV and $m_H = 70$ GeV; the dashed line is for $m_t = 100$ GeV and $m_H = 95$ GeV.

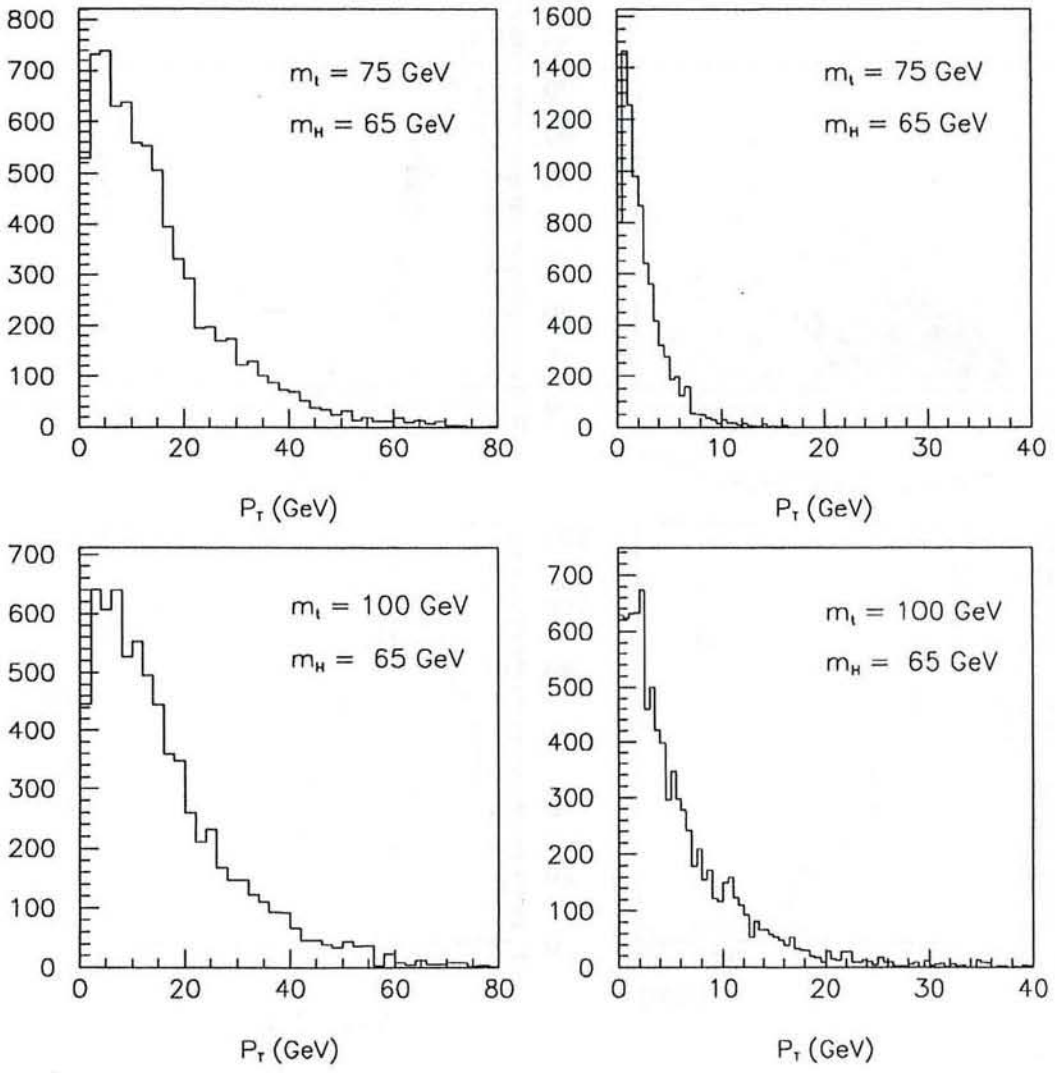

Figure : 6. The P_T distributions of leptons from the ISAJET Monte Carlo sample.
a) P_T of leptons from $H \rightarrow \tau\nu_\tau \rightarrow l$+X for $m_t = 75$ GeV and $m_H = 65$ GeV.
b) P_T of leptons from $b \rightarrow l$+X for $m_t = 75$ GeV and $m_H = 65$ GeV.
c) P_T of leptons from $H \rightarrow \tau\nu_\tau \rightarrow l$+X for $m_t = 100$ GeV and $m_H = 65$ GeV.
d) P_T of leptons from $b \rightarrow l$+X for $m_t = 100$ GeV and $m_H = 65$ GeV.

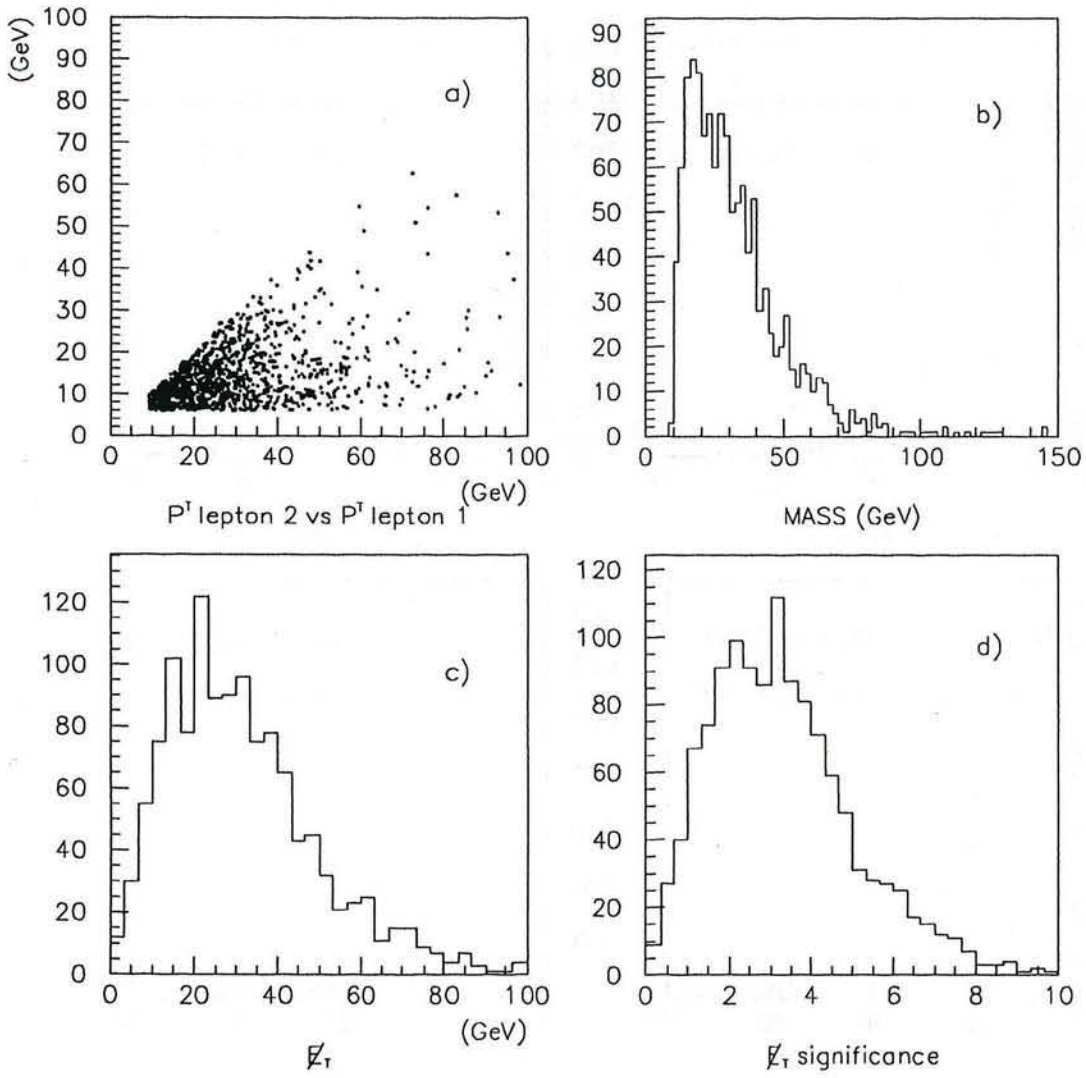

Figure : 7. Distributions of several reconstructed variables from the ISAJET Monte Carlo $t\bar{t} \rightarrow HbHb$ events, for m_t= 100GeV and m_H= 80GeV.
a) P_T^{l1}(highest lepton P_T) vs. P_T^{l2}(second highest lepton P_T)
b) Dilepton Invariant mass
c) Missing E_T
d) significance of $\not\!\!E_T$

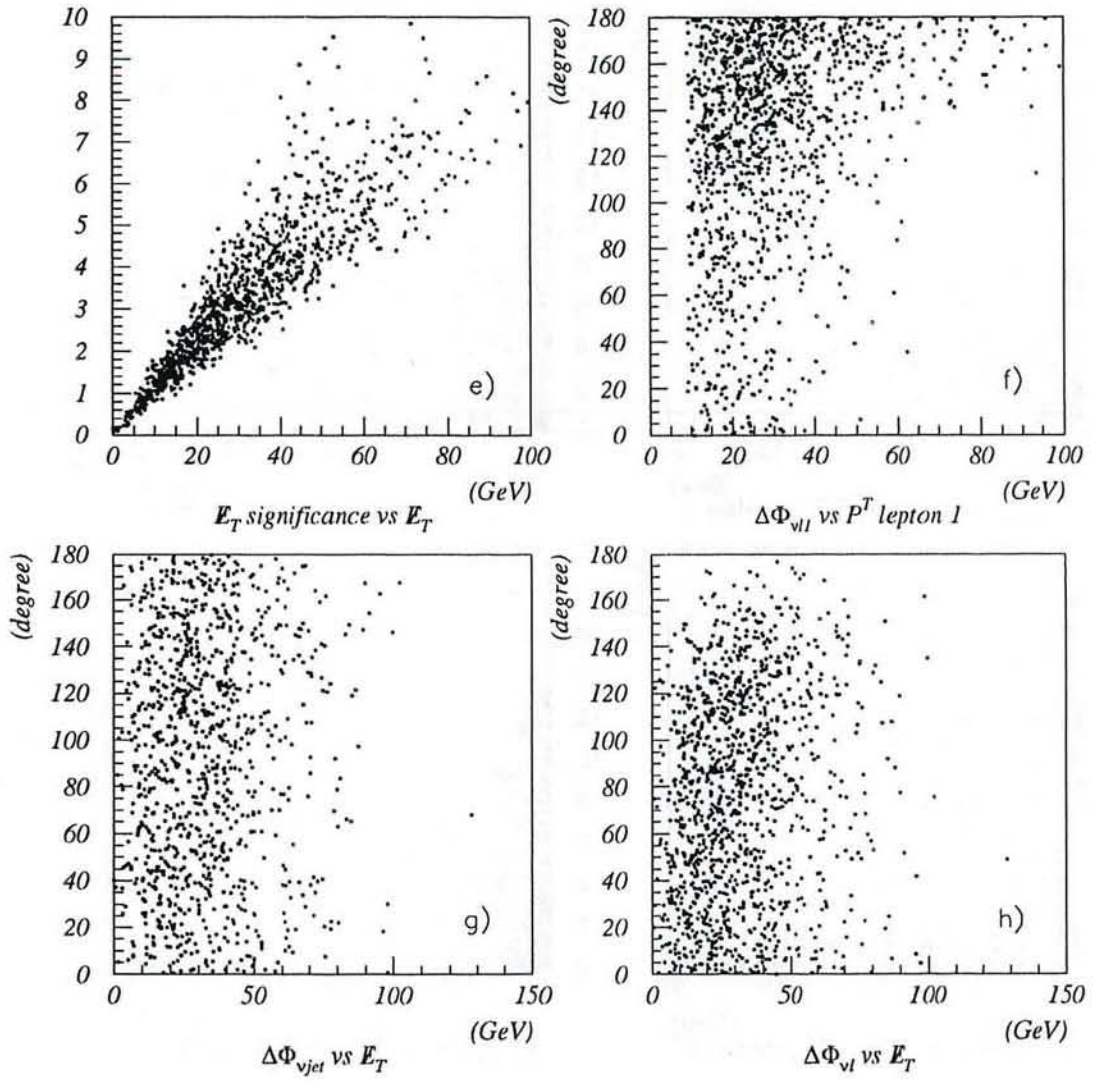

Figure : 7. Distributions of several reconstructed variables from the ISAJET Monte Carlo $t\bar{t} \rightarrow HbHb$ events, for m_t= 100 GeV and m_H= 80 GeV.
e) significance of $\not\!\!E_T$ vs. $\not\!\!E_T$
f) $\Delta\phi_{\nu l1}$($\Delta\phi$ between highest P_T lepton and $\not\!\!E_T$) vs. P_T^{l1}
g) $\Delta\phi_{\nu jet}$($\Delta\phi$ between the closest jet and $\not\!\!E_T$) vs. $\not\!\!E_T$
h) $\Delta\phi_{\nu l}$($\Delta\phi$ between the closest lepton and $\not\!\!E_T$) vs. $\not\!\!E_T$

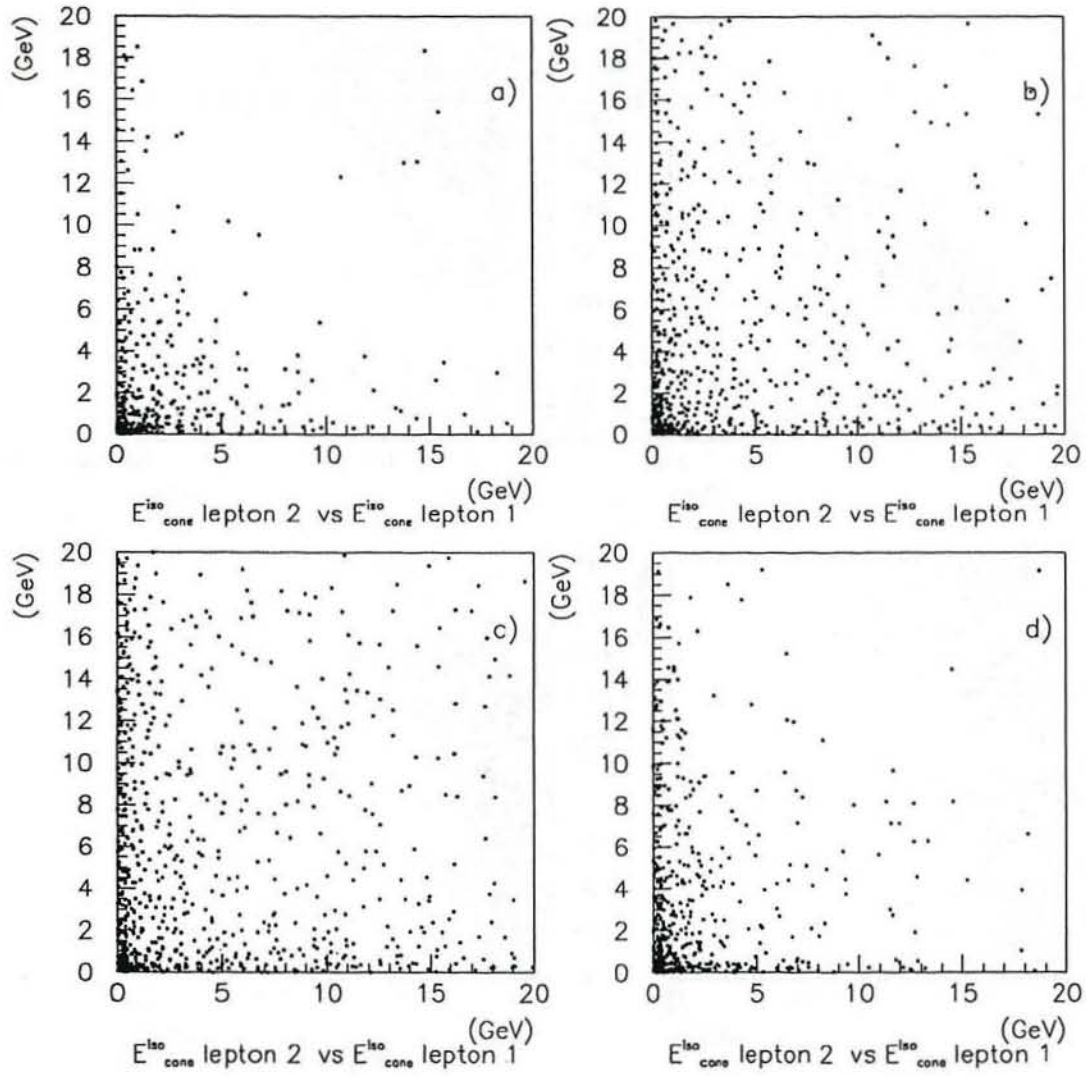

Figure : 8. Isolation distributions of Monte Carlo events for m_t= 100GeV.
E_{cone}^{iso} is the sum of E_T deposited in a cone of 0.4 around the lepton.
a) $t\bar{t} \rightarrow HbHb$, m_H= 95GeV
b) $t\bar{t} \rightarrow HbHb$, m_H= 80GeV
c) $t\bar{t} \rightarrow HbHb$, m_H= 65GeV
d) $t\bar{t} \rightarrow WbWb$

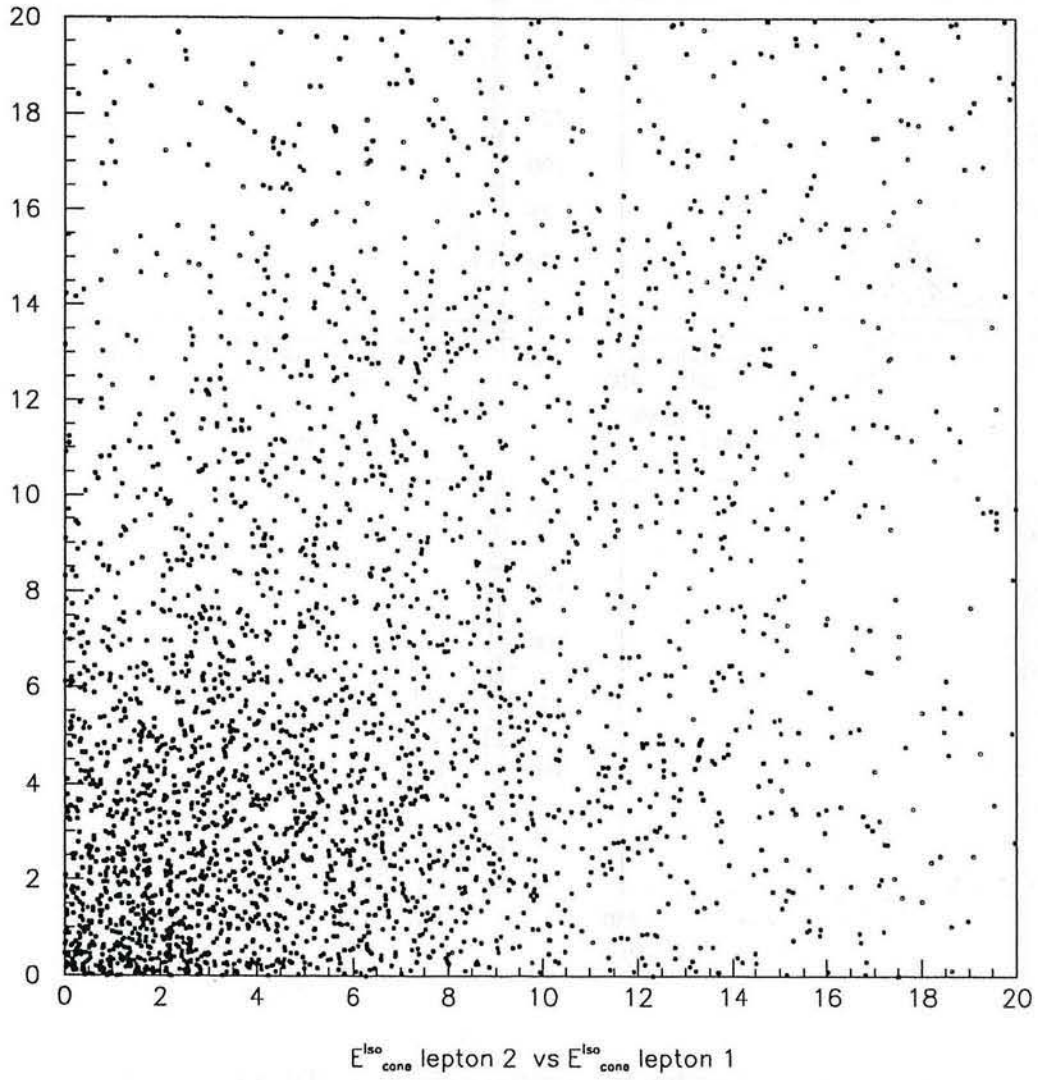

Figure : 9. Isolation distribution of the $b\bar{b}$ Monte Carlo events.

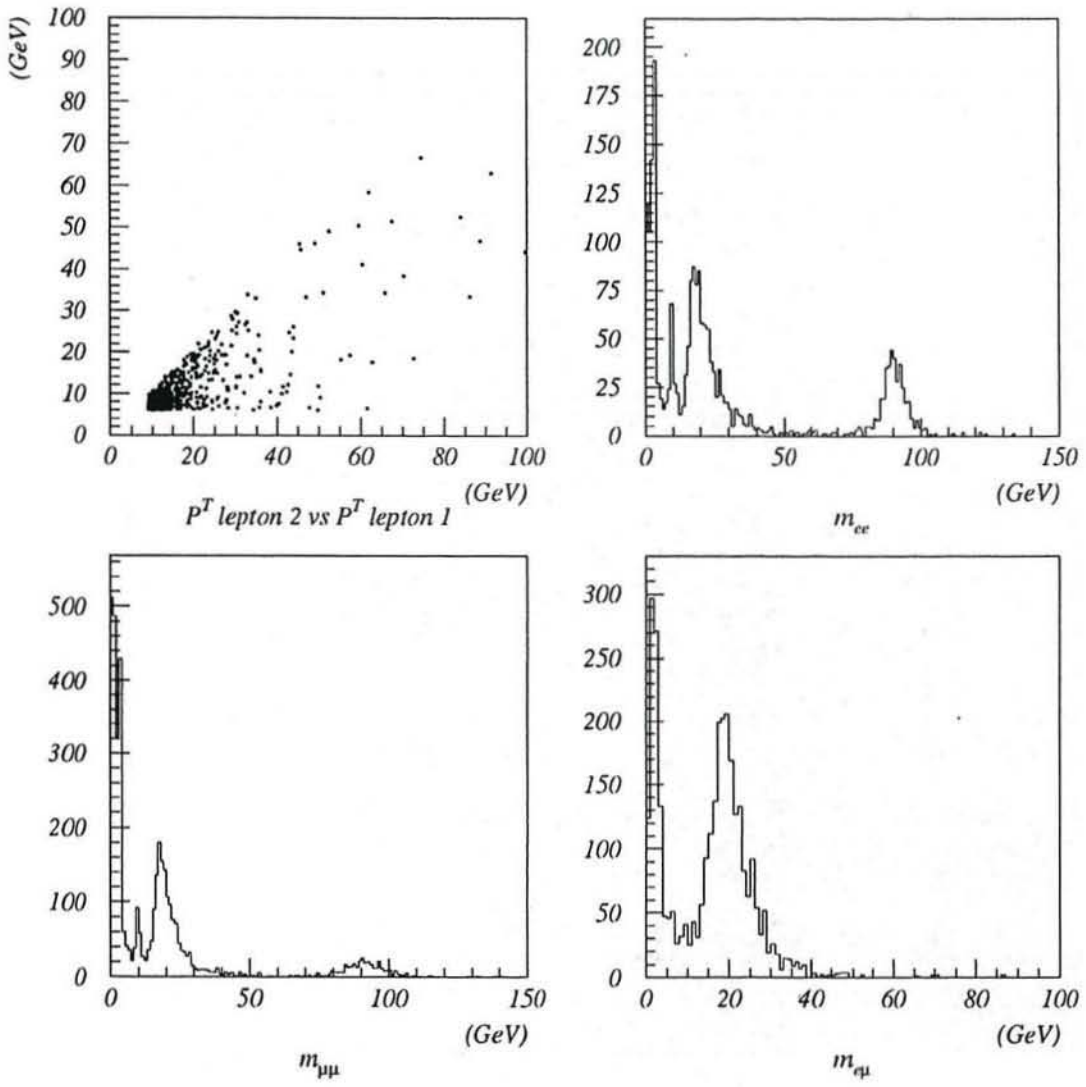

Figure : 10. P_T and invariant dilepton mass distributions of CDF run 1a data.
a) P_T^{l1} vs. P_T^{l2}
b) Invariant mass of ee events
c) Invariant mass of $\mu\mu$ events
d) Invariant mass of eμ events

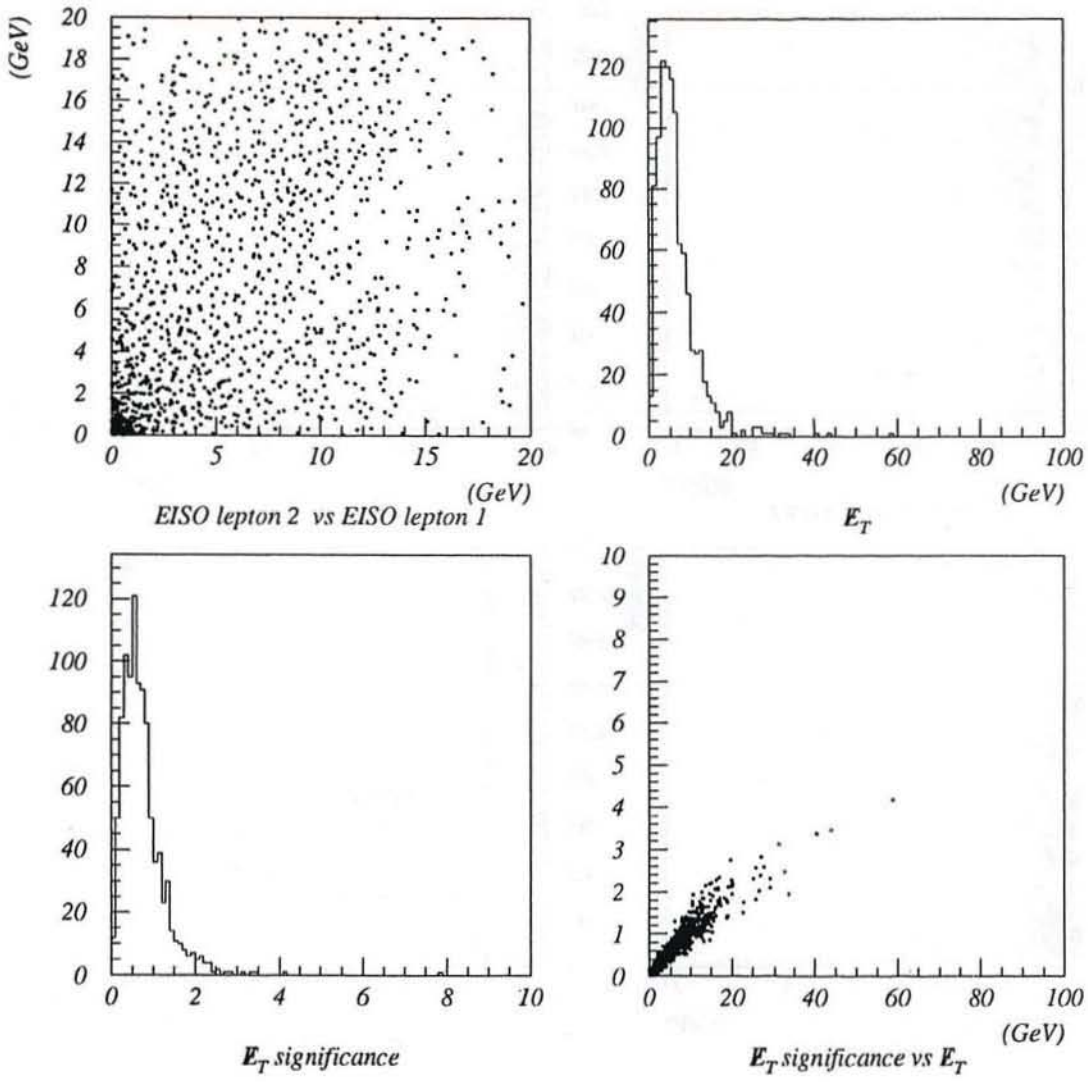

Figure : 11. Distributions of several variables from CDF run 1a data.
a) E_{cone}^{iso1} vs. E_{cone}^{iso2}
b) Missing E_T
c) significance of $\not\!\!E_T$
d) significance of $\not\!\!E_T$ vs. $\not\!\!E_T$

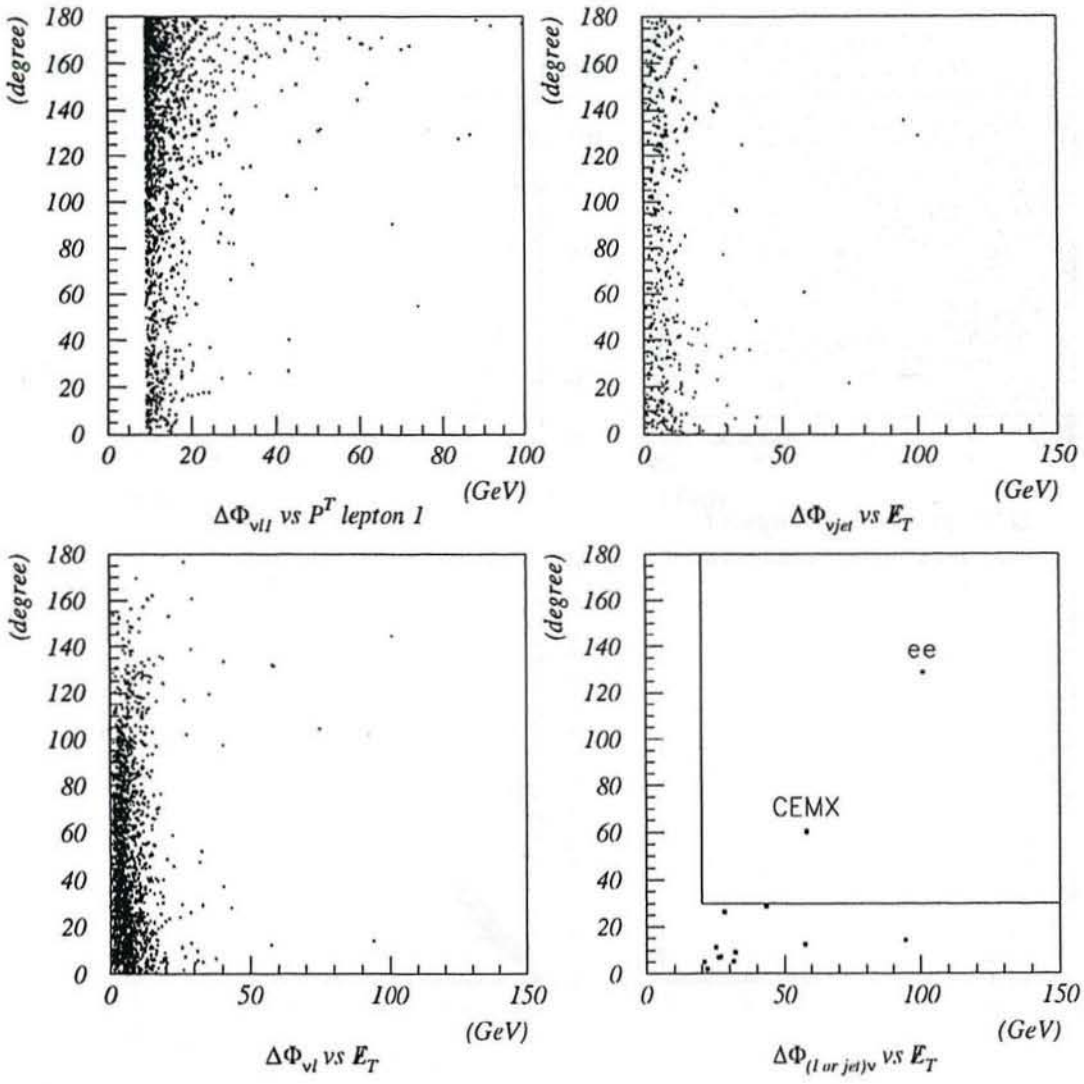

Figure : 11. Distributions of several variables from CDF run 1a data.
e) $\Delta\phi_{\nu l1}$ vs. P_T^{l1}
f) $\Delta\phi_{\nu jet}$ vs. $\not\!\!E_T$
g) $\Delta\phi_{\nu l}$ vs. $\not\!\!E_T$
h) $\Delta\phi$($\not\!\!E_T$-lepton or jet) vs. $\not\!\!E_T$ after isolation cut,mass cut, $\not\!\!E_T$> 20GeV cut, significance of $\not\!\!E_T > 2.4$ and W removal cut.

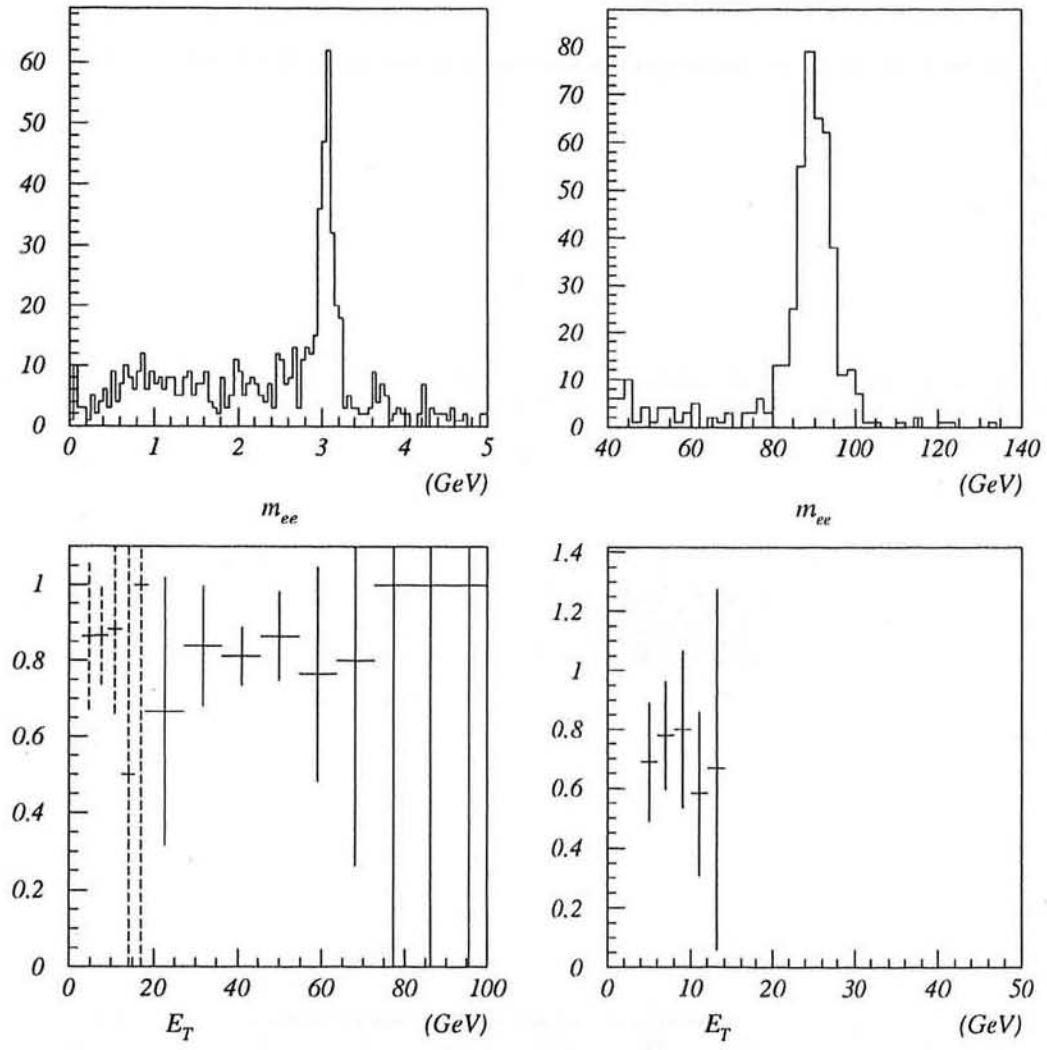

Figure : 12. Electron ID efficiencies.
a) Mass distribution of $J/\psi \rightarrow ee$
b) Mass distribution of $Z \rightarrow ee$
c) ID efficiency for isolated electrons vs. E_T of the electrons
d) ID efficiency for semi-isolated electrons vs. E_T of the electrons

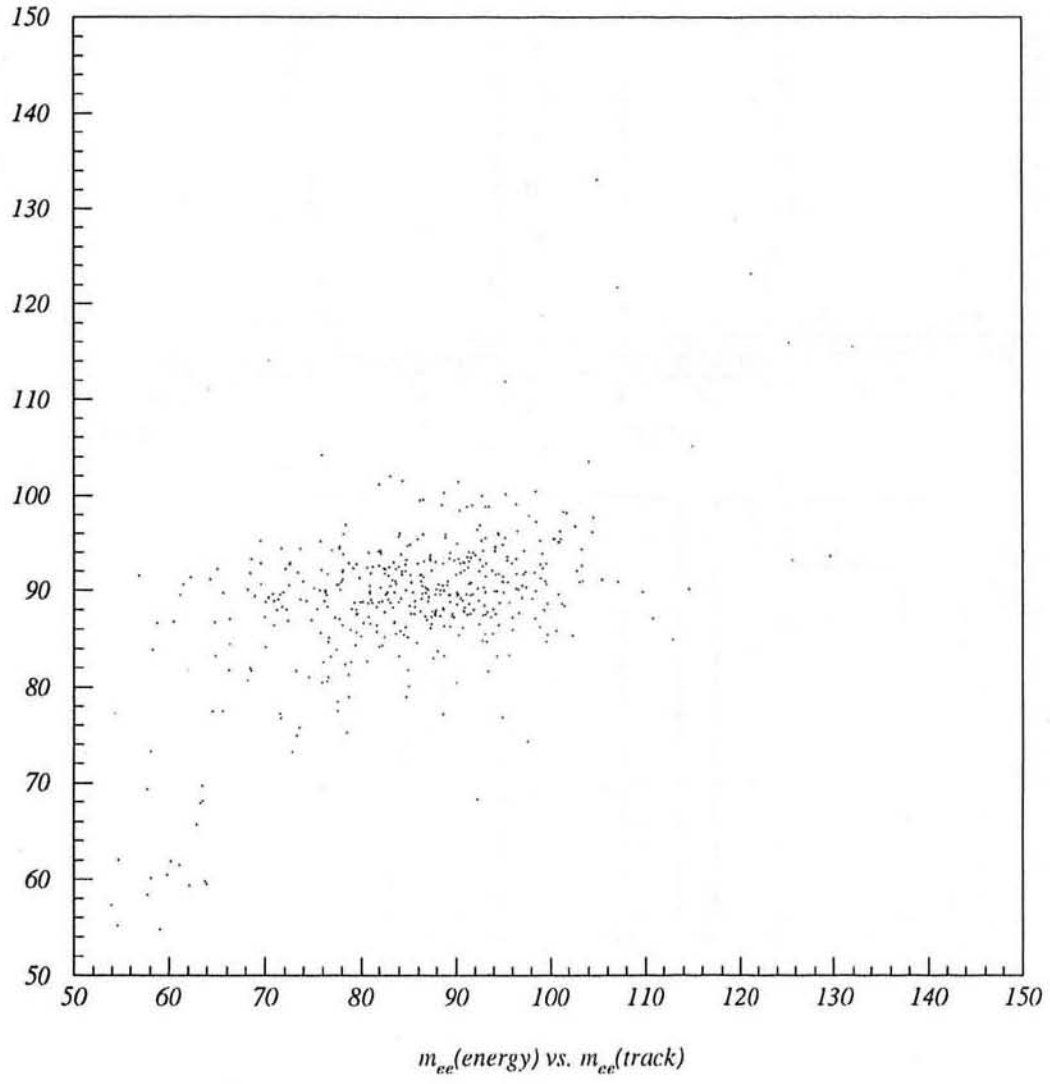

Figure : 13. Invariant mass of $Z \rightarrow ee$ calculated from electron energies vs. the invariant mass calculated from electron tracks for opposite sign electrons.

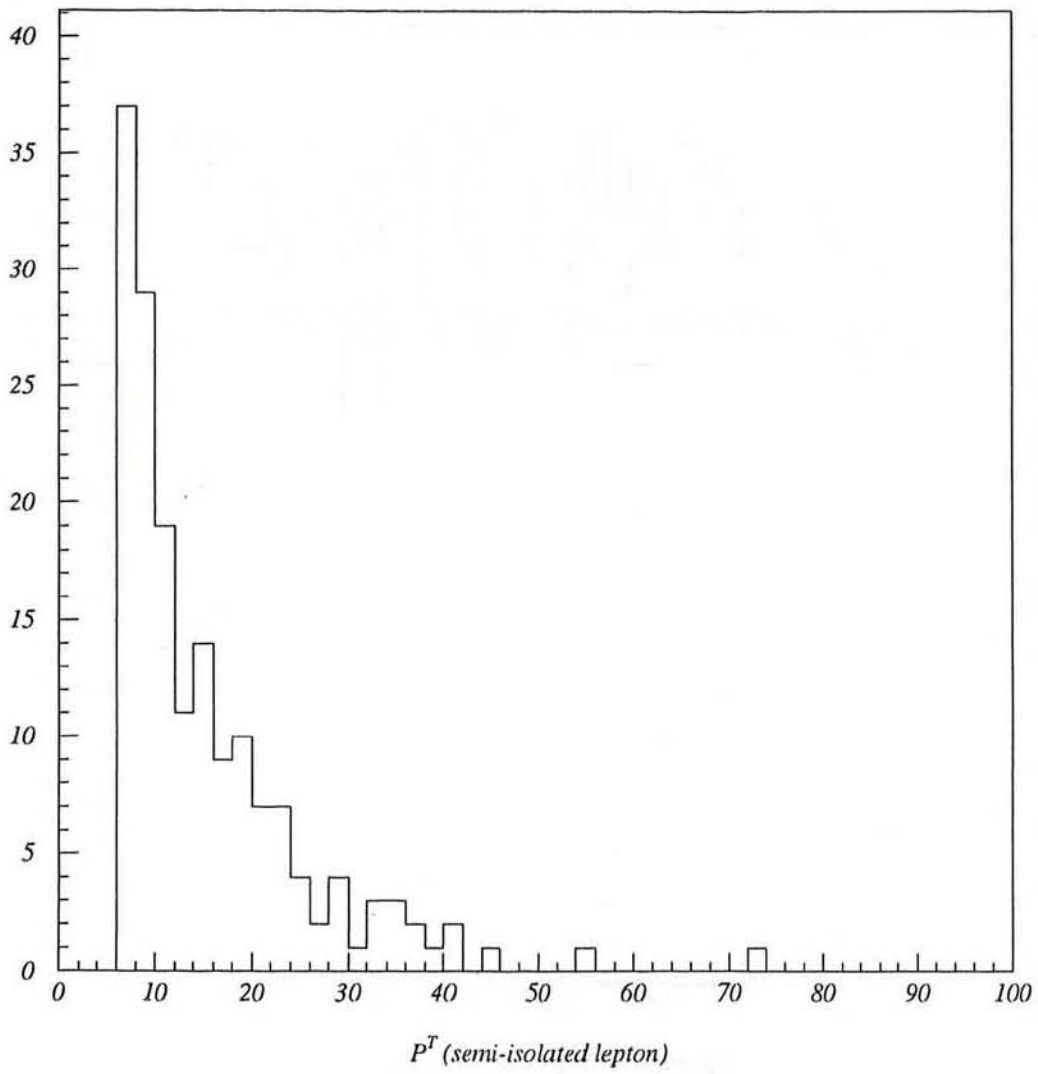

Figure : 14. P_T distribution of semi-isolated leptons for $m_t = 90$ GeV, $m_H = 55$ GeV from the ISAJET Monte Carlo.

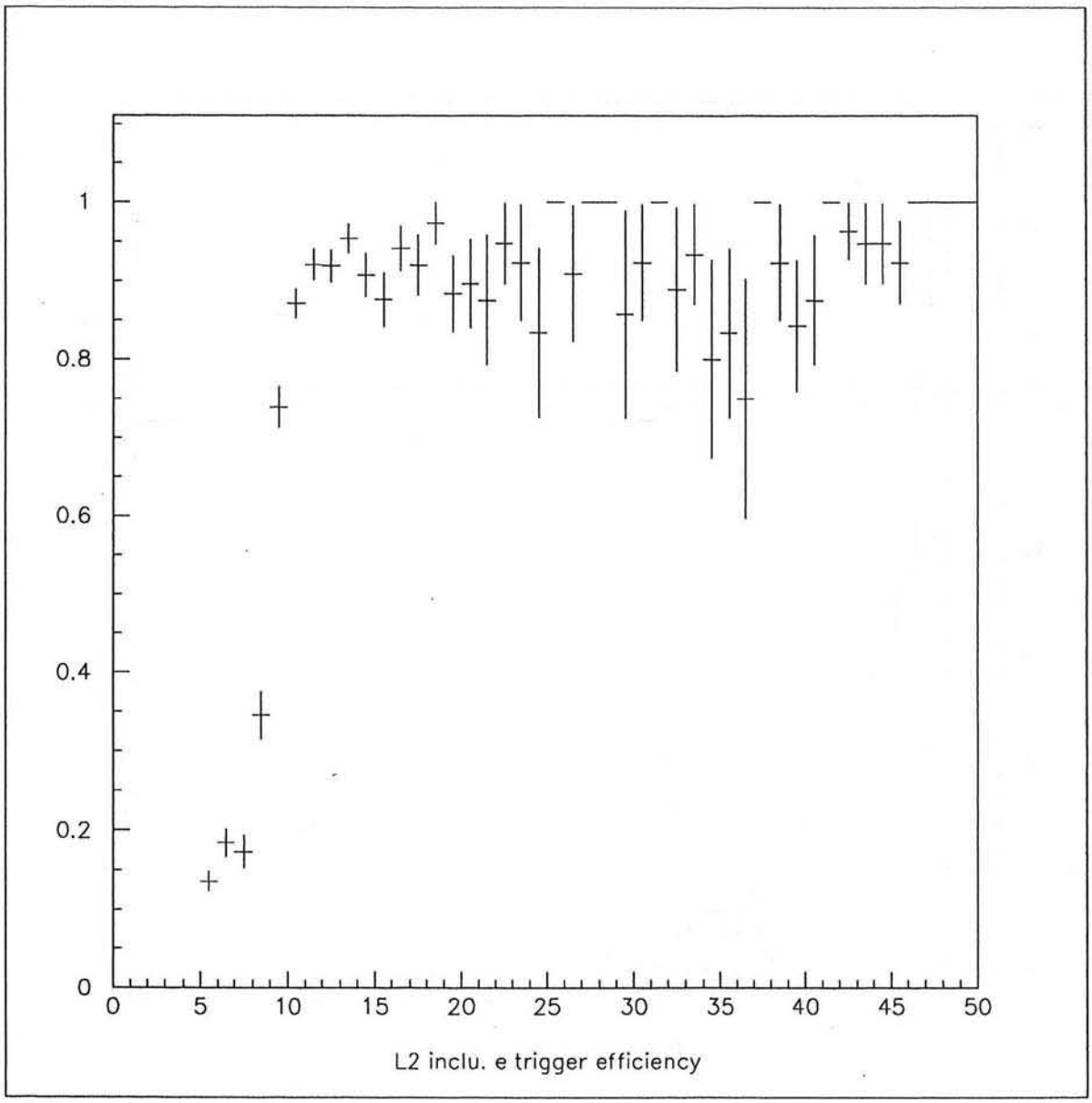

Figure : 15. Level 2 inclusive electron trigger efficiency

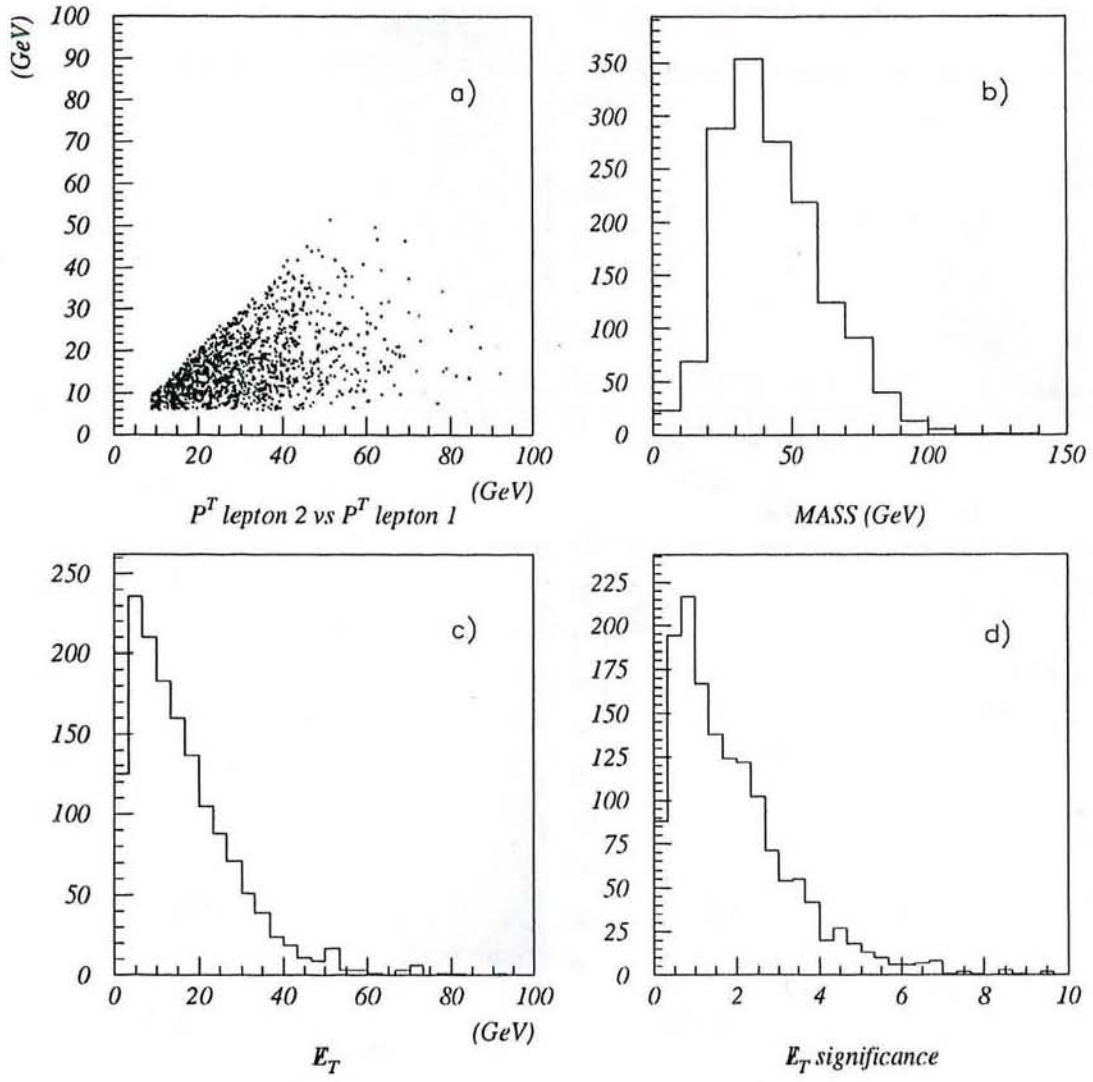

Figure : 16. Distributions of several variables from the $Z \rightarrow \tau\tau$ simulation sample.
a) P_T^{l1} vs. P_T^{l2}
b) Dilepton Invariant mass
c) Missing E_T
d) significance of $\not\!\!E_T$

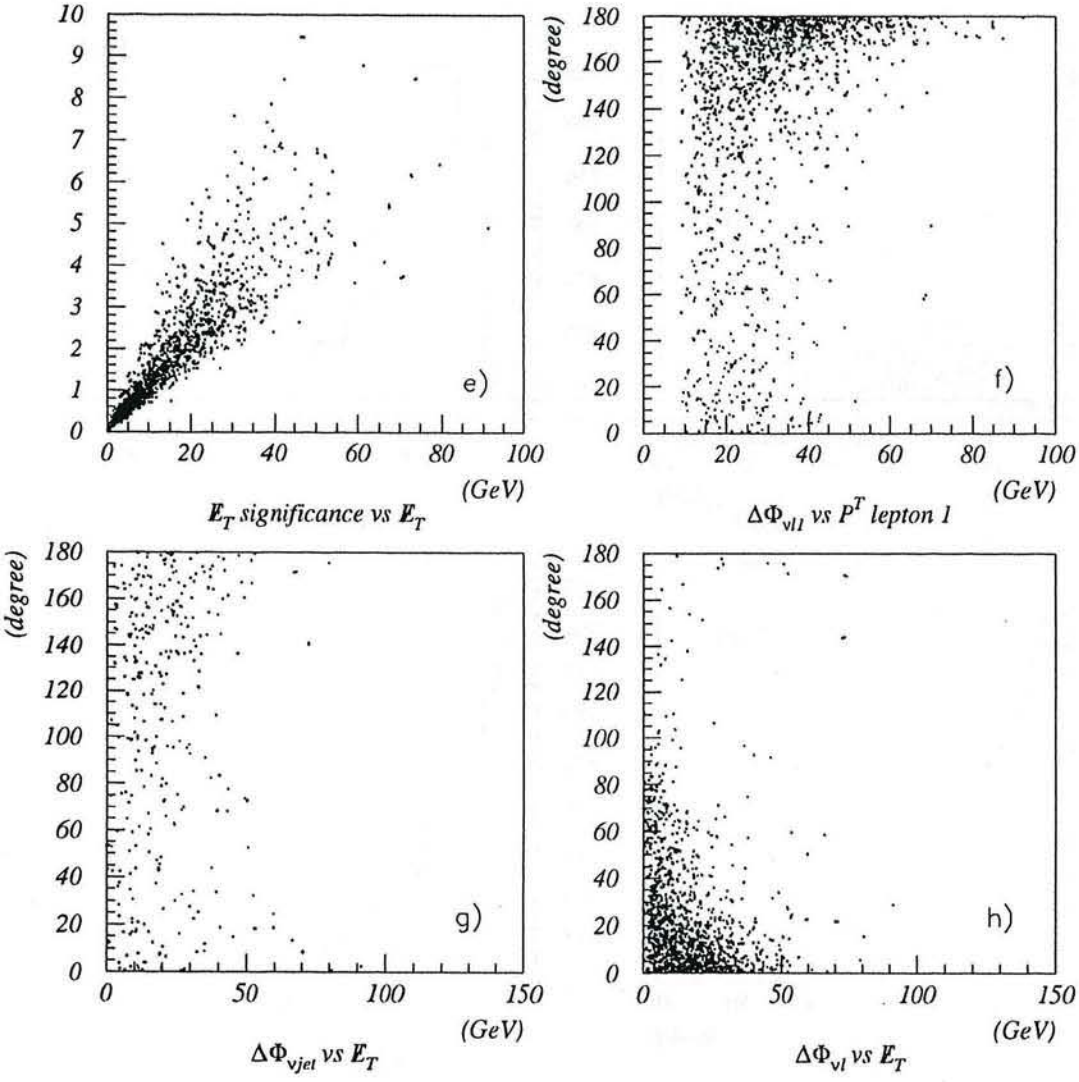

Figure : 16. Distributions of several variables from the $Z \rightarrow \tau\tau$ simulation sample.
e) significance of $\not\!\!E_T$ vs. $\not\!\!E_T$
f) $\Delta\phi_{\nu l1}$ vs. P_T^{l1}
g) $\Delta\phi_{\nu jet}$ vs $\not\!\!E_T$
h) $\Delta\phi_{\nu l}$ vs $\not\!\!E_T$

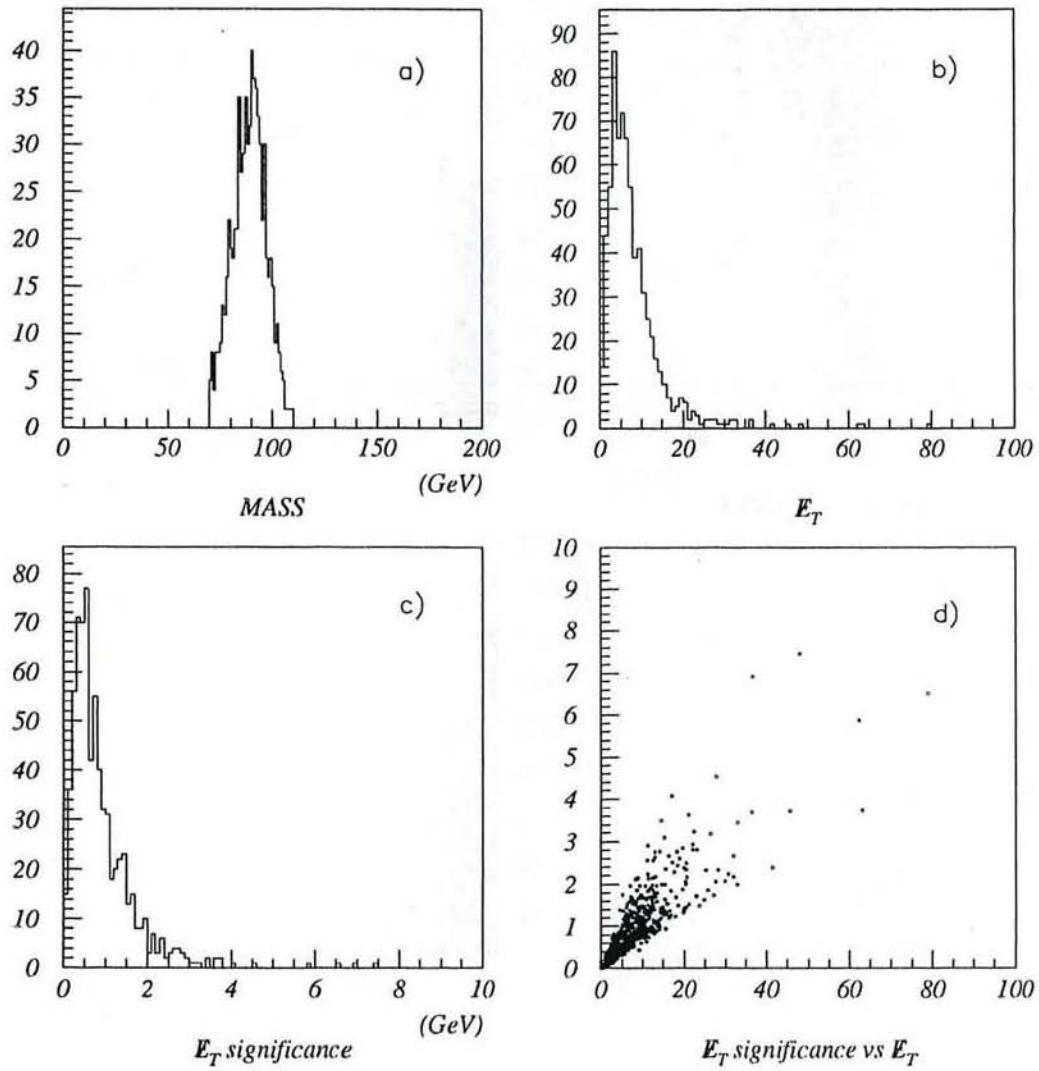

Figure : 17. Distributions of several variables from the $Z \rightarrow ee$ and $Z \rightarrow \mu\mu$ data samples.
a) Dilepton Invariant mass
b) Missing E_T
c) significance of $\not\!\!E_T$
d) significance of $\not\!\!E_T$ vs. $\not\!\!E_T$

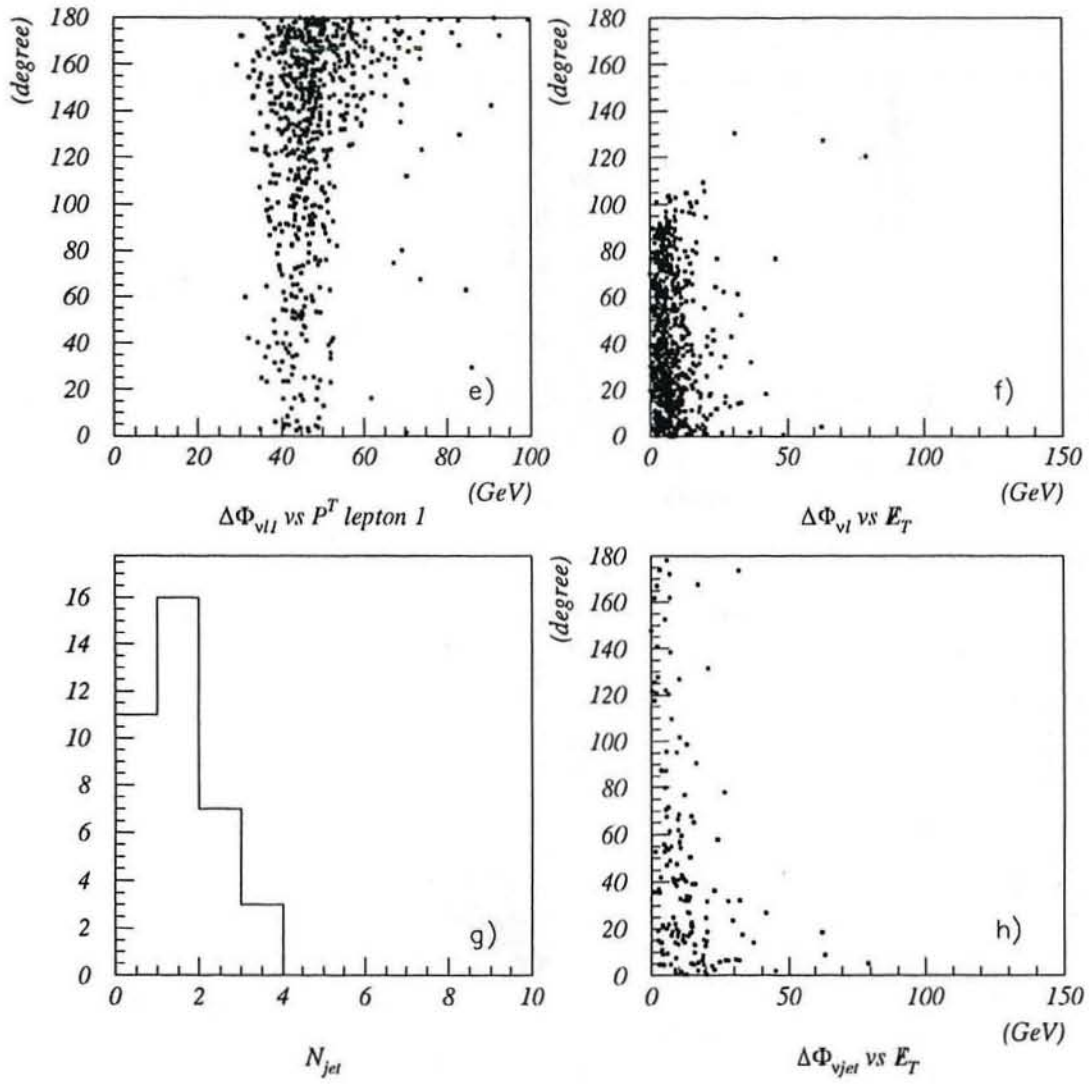

Figure : 17. Distributions of several variables from the $Z \rightarrow ee$ and $Z \rightarrow \mu\mu$ data samples.
e) $\Delta\phi_{\nu l1}$ vs. P_T^{l1}
f) $\Delta\phi_{\nu l}$ vs $\not\!\!E_T$
g) Number of jet distribution after $\not\!\!E_T > 20$ GeV cut
h) $\Delta\phi_{\nu jet}$ vs $\not\!\!E_T$

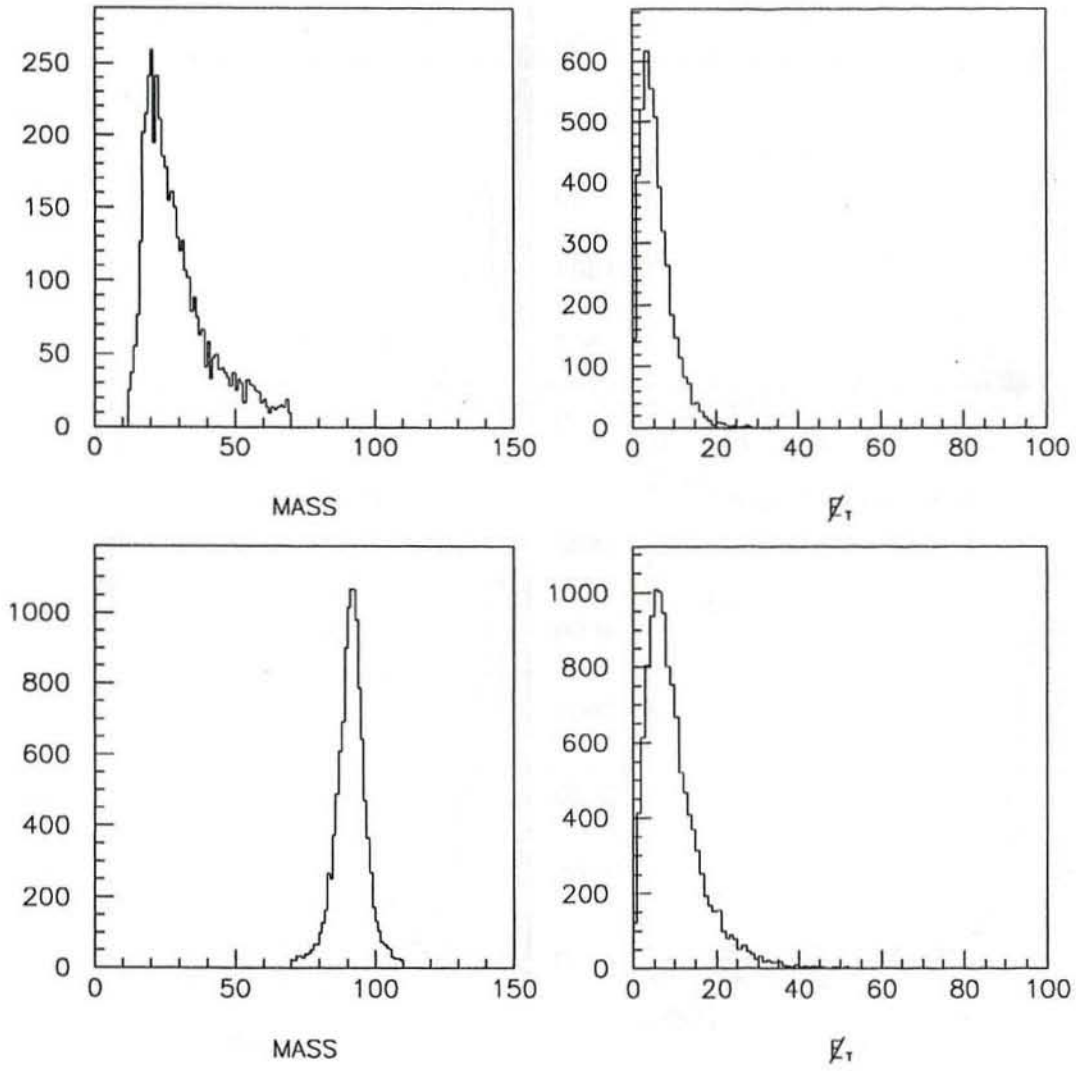

Figure : 18. Invariant mass and $\not\!\!E_T$ distributions for different Drell-Yan mass regions.
a) Invariant mass of low mass Drell-Yan(12-70 GeV)
b) $\not\!\!E_T$ of low mass Drell-Yan(12-70 GeV)
c) Invariant mass of Z for our cut(70-110 GeV)
d) $\not\!\!E_T$ of Z for our cut(70-110 GeV)

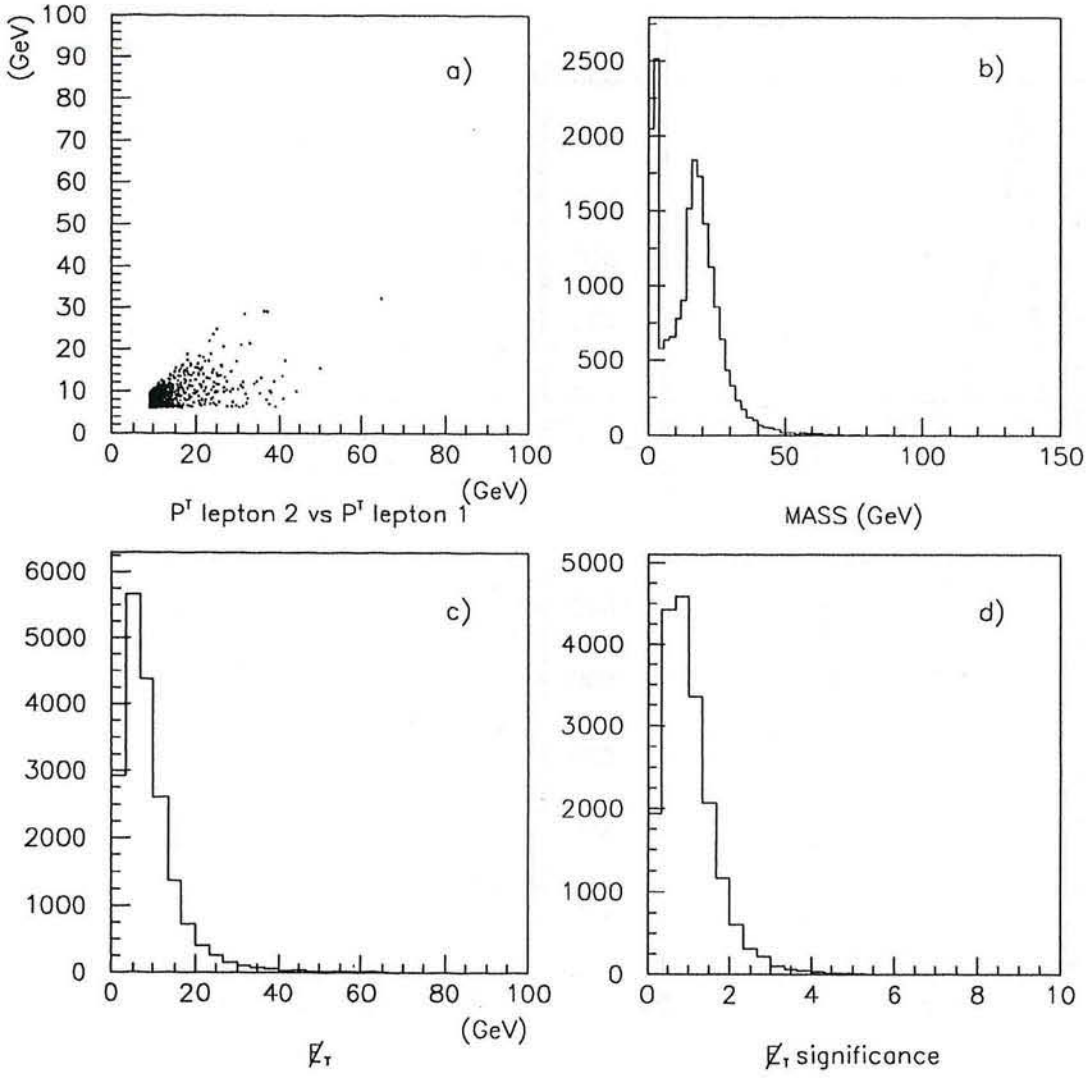

Figure : 19. Distributions of several variables from the $b\bar{b}$ Monte Carlo sample.
a) P_T^{l1} vs. P_T^{l2}
b) Dilepton Invariant mass
c) Missing E_T
d) significance of $\not\!\!E_T$

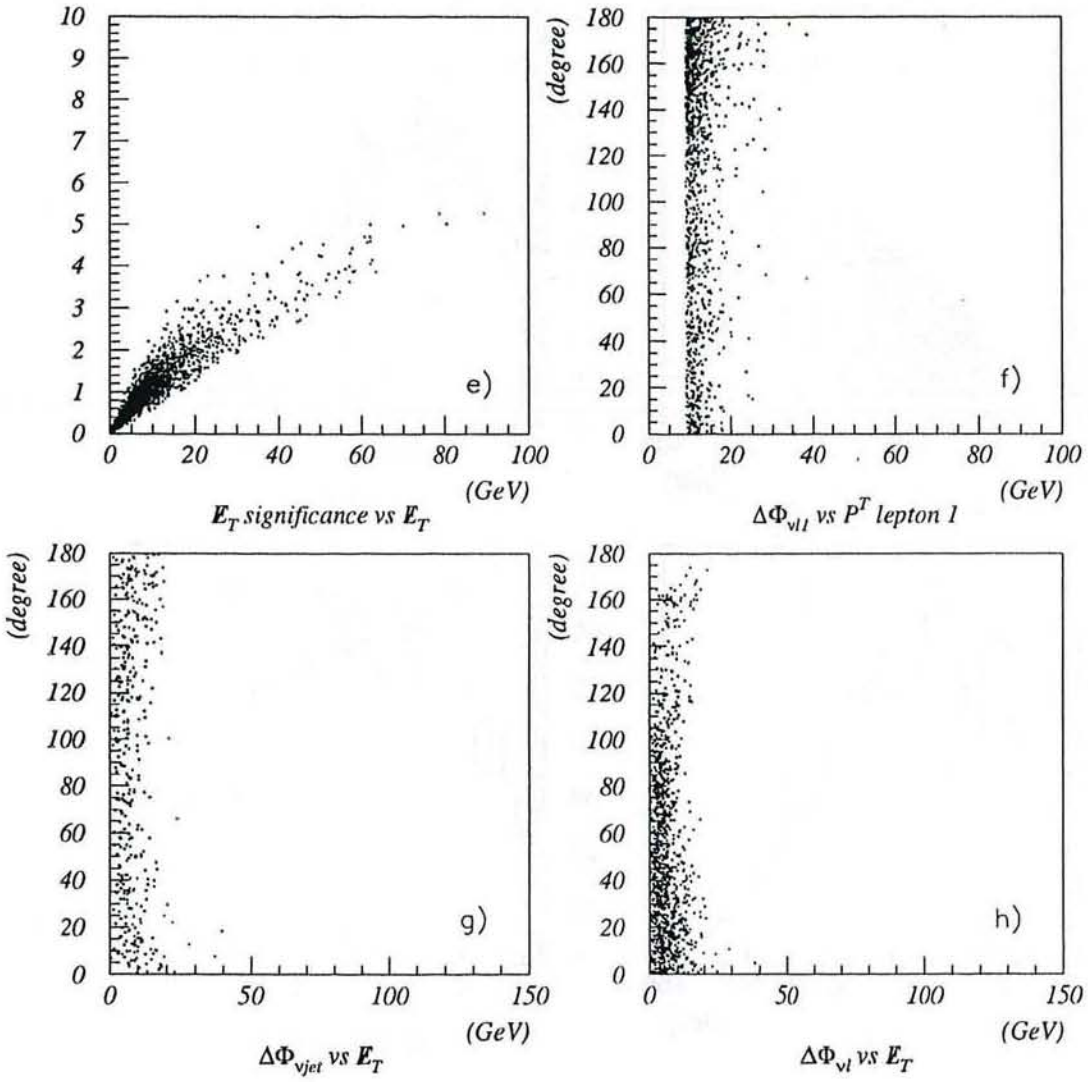

Figure : 19. Distributions of several variables from the $b\bar{b}$ Monte Carlo sample.
e) significance of $\not\!\!E_T$ vs. $\not\!\!E_T$
f) $\Delta\phi_{\nu l1}$ vs. P_T^{l1}
g) $\Delta\phi_{\nu jet}$ vs $\not\!\!E_T$
h) $\Delta\phi_{\nu l}$ vs $\not\!\!E_T$

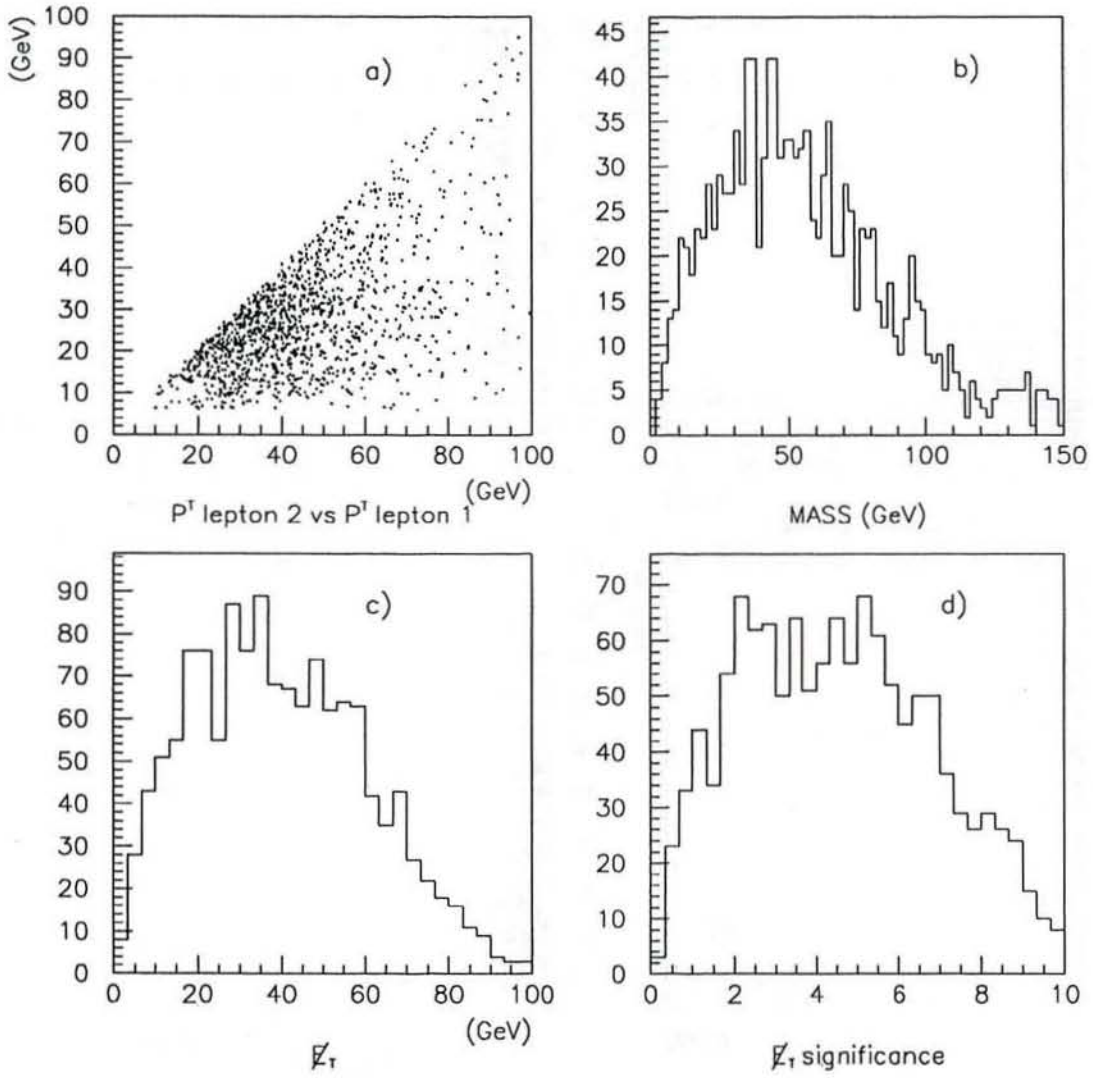

Figure : 20. Distributions of several variables from the WW Monte Carlo sample.
a) P_T^{l1} vs. P_T^{l2}
b) Dilepton Invariant mass
c) Missing E_T
d) significance of $\not\!\!E_T$

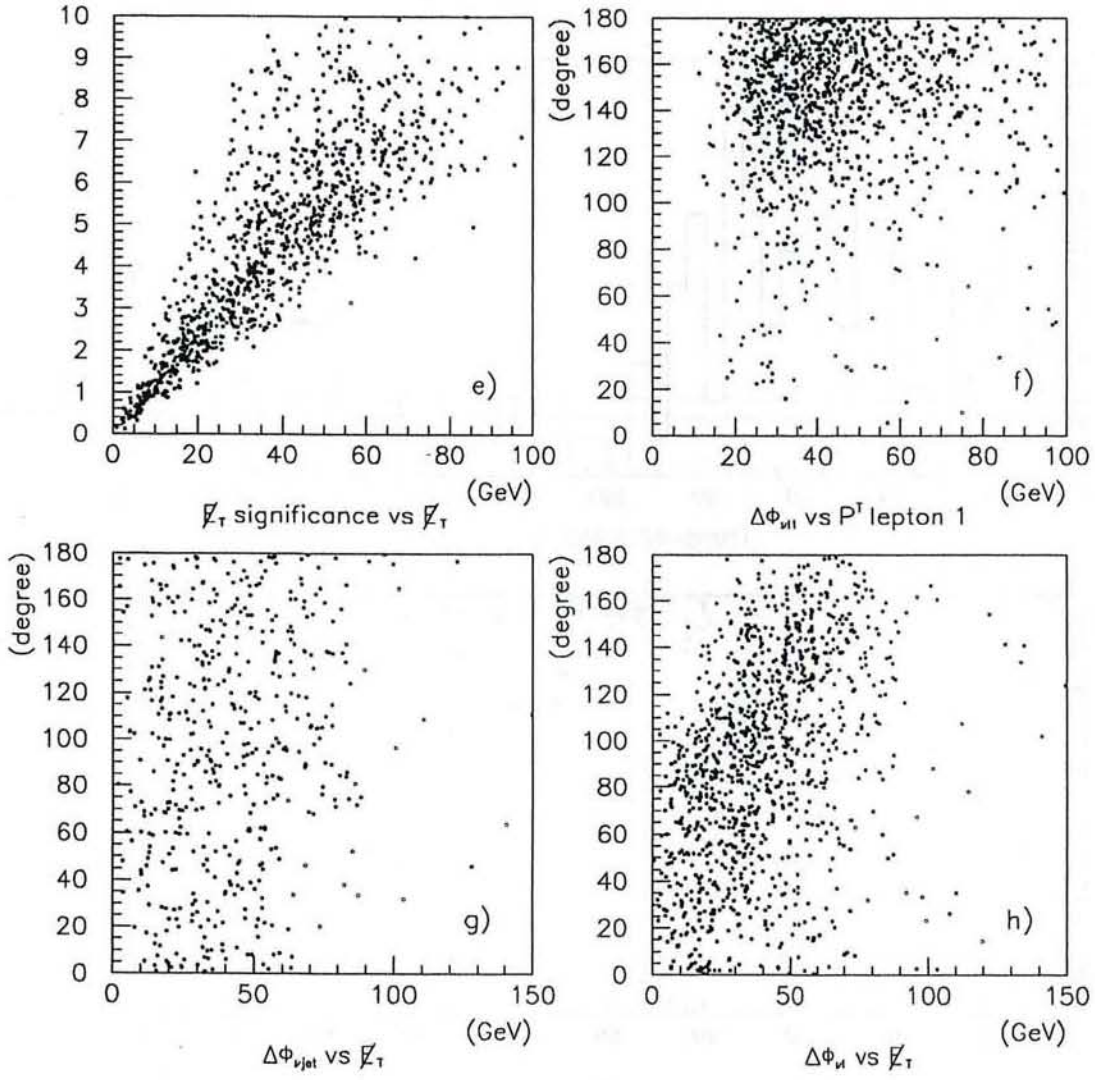

Figure : 20. Distributions of several variables from the WW Monte Carlo sample.
e) significance of $\not\!\!E_T$ vs. $\not\!\!E_T$
f) $\Delta\phi_{\nu l1}$ vs. P_T^{l1}
g) $\Delta\phi_{\nu jet}$ vs $\not\!\!E_T$
h) $\Delta\phi_{\nu l}$ vs $\not\!\!E_T$

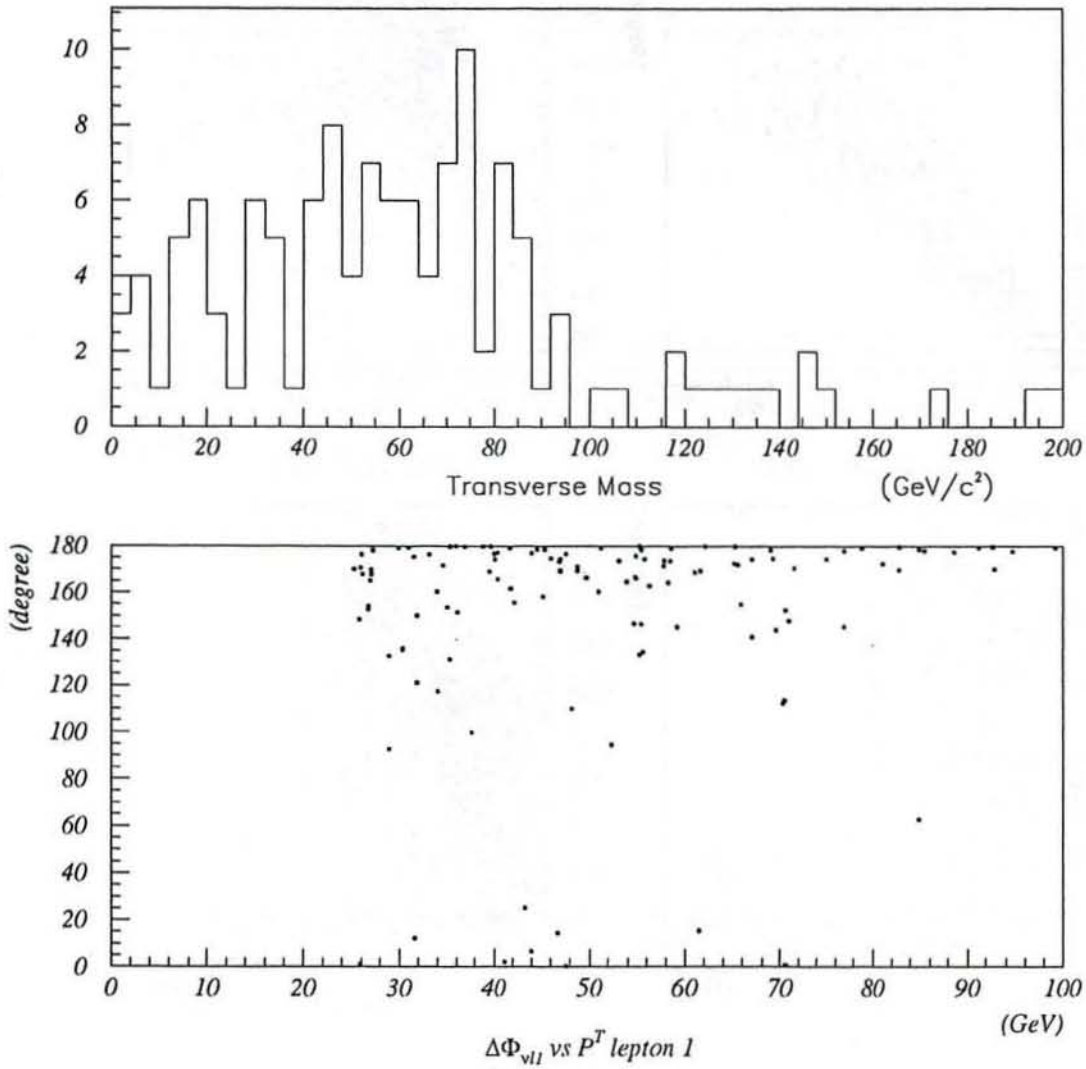

Figure : 21. Distribution of variables from W + jets data sample.
a) Transverse mass of $\not\!\!E_T$ and P_T^{l1}.
b) $\Delta\phi_{\nu l1}$ vs. P_T^{l1}

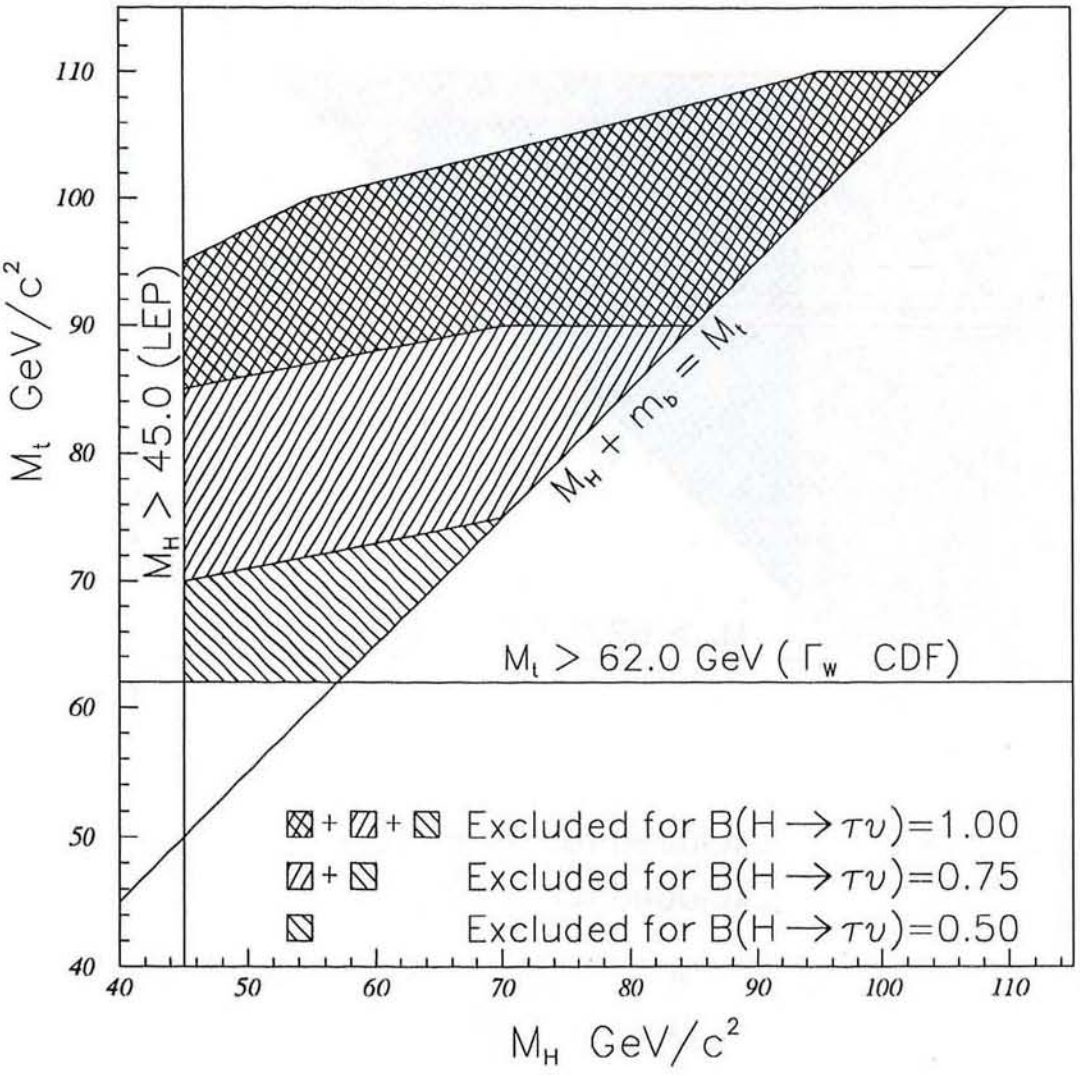

Figure : 22. Regions of (m_t, m_H) plane excluded at 95% CL. for Br($t \rightarrow H^+ b$)=1.0

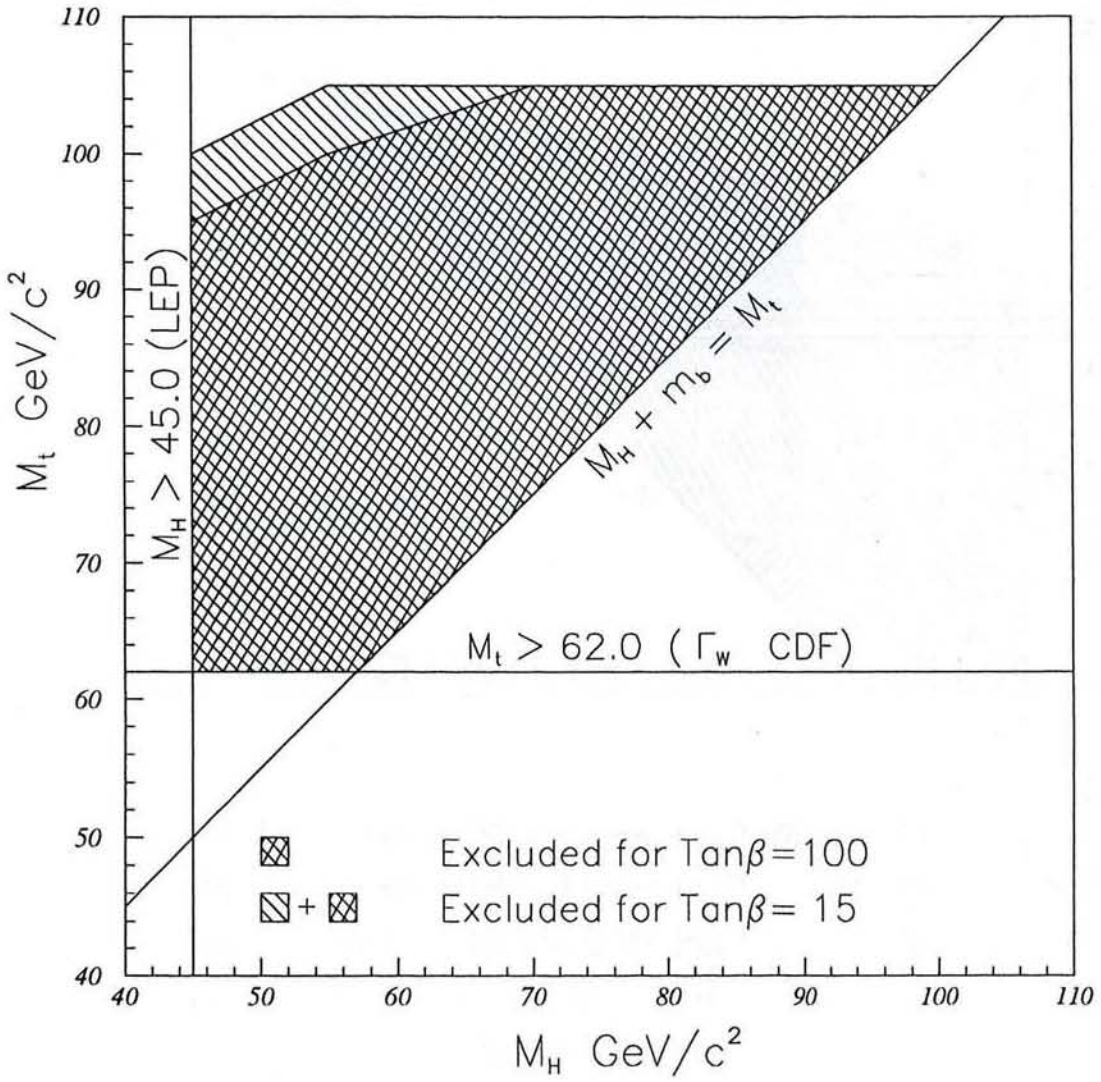

Figure : 23. Regions of (m_t,m_H) plane excluded at 95% CL. for THD model